# 3. Results

## 3.1. Immunostimulation and characterisation of the active compound GLIS from *Ganoderma lucidum*

### 3.1.1. Activation of macrophages by GLIS

#### 3.1.1.1. Activation of bone marrow-derived macrophages (BMMs) by different fungi crude extracts and by GLIS

LZ, YZ, HSH, HT and LZSBS were the crude extracts isolated from the fruit bodies of *Ganoderma lucidum*, *Coriolus versicolor*, *Hericium erinaceum*, *Grifola frondosa* and the spore of *Ganoderma lucidum*, respectively. The response of macrophages to these different fungi crude extracts was measured. It was found (Fig. 1A) that all five crude extracts activated BMMs in the range of 5 –100 µg/ml. Among them, LZ appeared to be the most active extract for macrophage activation.

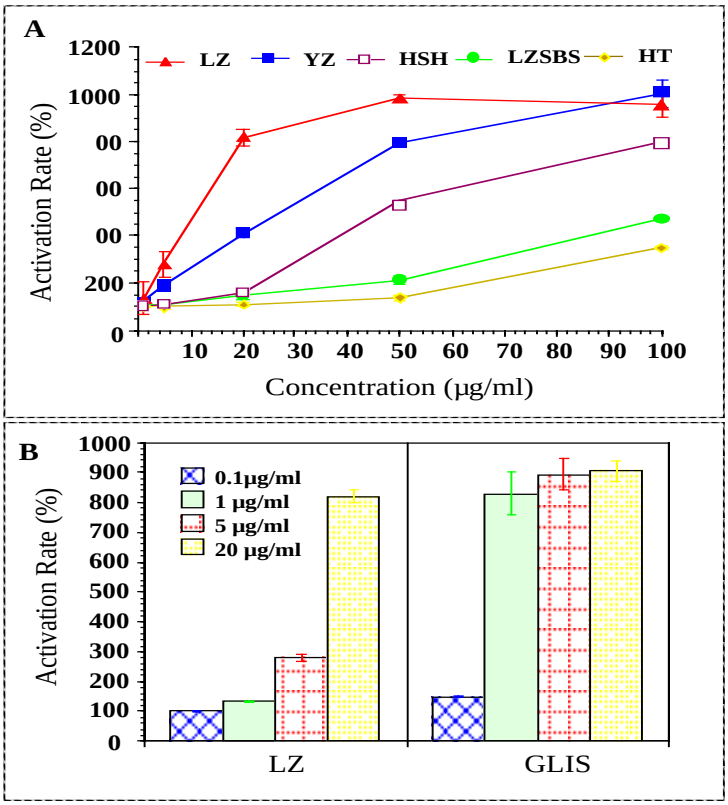


Fig. 1. Activation of macrophages by the crude extracts or GLIS. BMMs were *in vitro* treated with different concentration of five fungal crude extracts LZ, YZ, HT, HSH and LZSBS (A), LZ or GLIS (B) for 72 h. The activation rate was measured by Alamar Blue Assay. Results present means ± SD of triplicates of one representative experiments.

Previous works have shown that LZ could also stimulate mouse lymphocytes. With bioassay-directed fractionation, an active fraction GLIS was isolated from the crude extract of LZ by several chromatographic steps. GLIS is a proteoglycan and has a carbohydrate:protein ratio of 11.5:1 (Zhang, 2000).

Fig. 1B presents the effect of GLIS isolated from LZ on macrophages in comparison with that of LZ. Both GLIS and LZ induced activation of macrophages, but the concentration of GLIS achieving the same activation rate was only one-twentieth that of LZ. The result suggests that GLIS is the active fraction for the activation of macrophages in the crude extract of LZ.

#### 3.1.1.2. Activation of macrophages from normal mice (BMMs) and tumour mice (TBMMs) by GLIS

In the presence of GLIS at the dose of 1 μg/ml, morphological changes in cultured BMMs were detectable after 24 h (Fig. 2A). The cells were more spread out and elongated than those of controls. No toxicity was found in cultures treated with GLIS at the dose of 0.1-1000 μg/ml as determined by microscopic examination and trypan blue exclusion test.

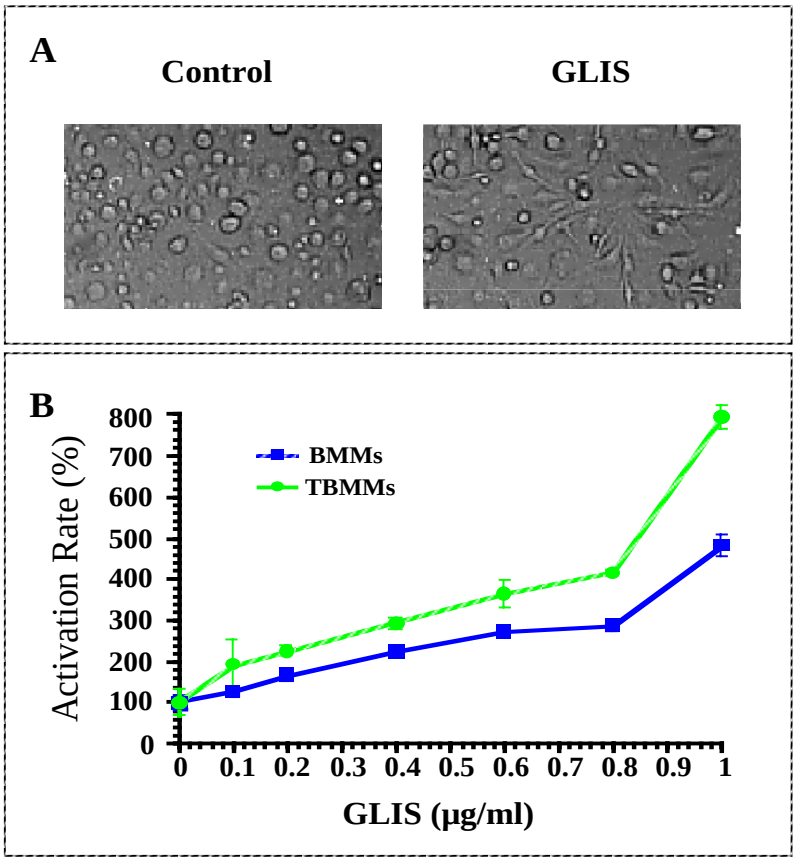


Fig. 2. Activation of macrophages by GLIS. (A) Morphological change of BMMs *in vitro* after stimulation by GLIS (1 μg/ml) for 24 h. (B) Activation of BMMs and TBMMs stimulated with different concentration of GLIS *in vitro* for 72 h. Results present means ± SD of triplicates of one representative experiments.

Usually the immune response is reduced in a tumour-bearing host. In order to study whether immunoresponse could be improved by GLIS, the response of bone marrow-derived macrophages from either normal mice (BMMs) or tumour mice (TBMMs) were compared. Both BMMs and TBMMs were activated by GLIS in a dose dependent manner in the range of 0.1-1 μg/ml; however, TBMMs were more sensitive to the stimulus of GLIS than BMMs.

### 3.1.1.3. Increase of interleukin-1β (IL-1β) and tumour necrosis factor-α (TNF-α) secretion of BMMs and TBMMs stimulated by GLIS

In the experiments mentioned above, it was found that GLIS was able to activate macrophages. The activation of macrophages allows for the production of many immunomodulatory substances, for example, cytokines. The ability of GLIS to induce IL-1β and TNF-α secretion, which are currently assumed to be the primary mediators involved in the killing of tumour cells, was examined.

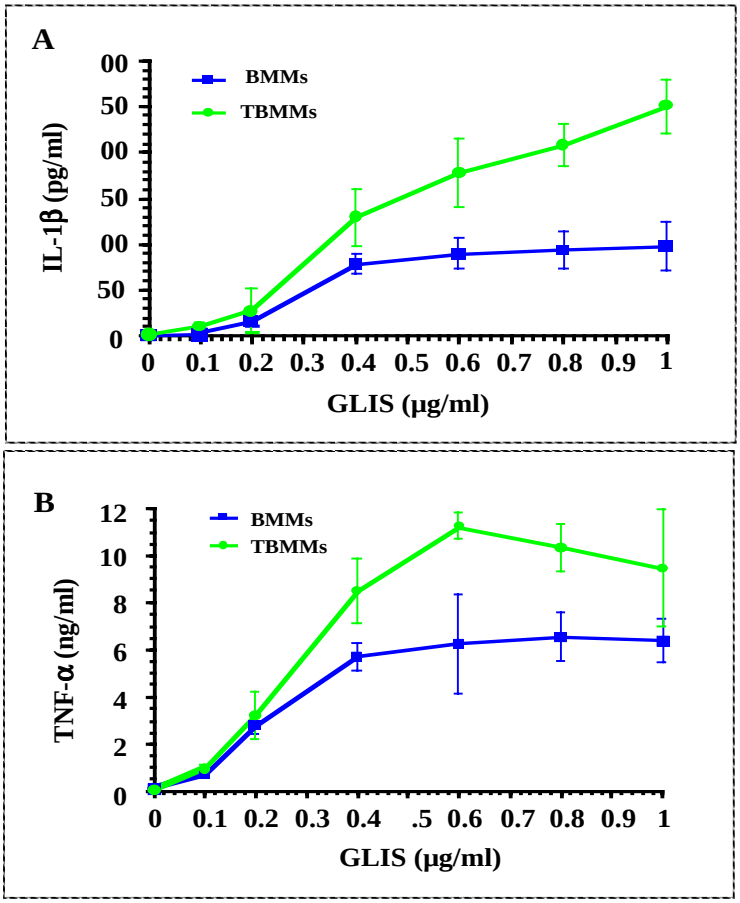


Fig. 3. Secretion of cytokine by macrophages after stimulation by GLIS. BMMs and TBMMs were incubated with different concentration of GLIS (0.1-1 μg/ml) *in vitro*. Culture supernatants were harvested after 24 h and assayed for concentrations of IL-1β (A) and TNF-α (B). Results present means ± SD of 3 different experiments.

Figs. 3A and 3B illustrate the increased secretion of cytokine IL-1β and TNF-α of BMMs and TBMMs after exposure to GLIS. GLIS induced a dose-dependent increase of IL-1β and TNF-α secretion. However, the amount of IL-1β and TNF-a secretion by TBMMs was significantly higher than that of BMMs after exposure to GLIS.

### 3.1.1.4. Production of reactive nitrogen intermediates (RNI) by BMMs and TBMMs after stimulation with GLIS

Reactive nitrogen intermediates (RNI) are important for macrophage tumouricidal activity. The level of RNI was determined by the amount of nitrite ($NO_2$) that is a stable metabolite of RNI. In this experiment, after macrophages were stimulated with GLIS for 24 h, RNI generation by BMMs and TBMMs was enhanced significantly in a dose dependent manner. The production of RNI by TBMMs in the presence of GLIS was markedly higher than that by BMMs (Fig. 4).

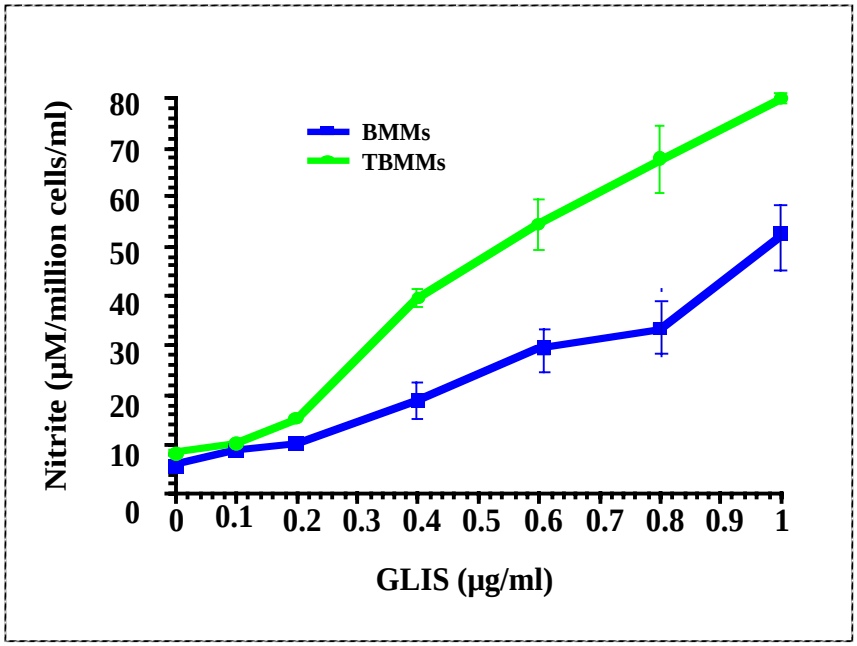


Fig. 4. Production of reactive nitrogen intermediates by macrophages treated by GLIS. BMMs and TBMMs were stimulated with different concentration of GLIS (0.1-1.0 μg/ml) for 24 h *in vitro*. The supernatants were harvested and assayed for reactive nitrogen intermediates. Results present means ± SD of 3 different experiments.

### 3.1.1.5. Increase of phagocytosis of BMMs and TBMMs after stimulation by GLIS

One of the prominent features of macrophages is to ingest and destroy inhaled particulate matter by phagocytosis. Morphological changes were found after macrophages were treated with GLIS in the presence of latex beads for 24 h. Most of the cells were able to take up latex beads. Only a few of the control cells, treated without GLIS, had this capacity (Fig.5A). The percentages of phagocytic cells were counted microscopically. GLIS could enhance the

percentage of BMMs phagocytic cells from 17% to 90% and of TBMMs from 35% to 90% (Figs. 5B and 5C).

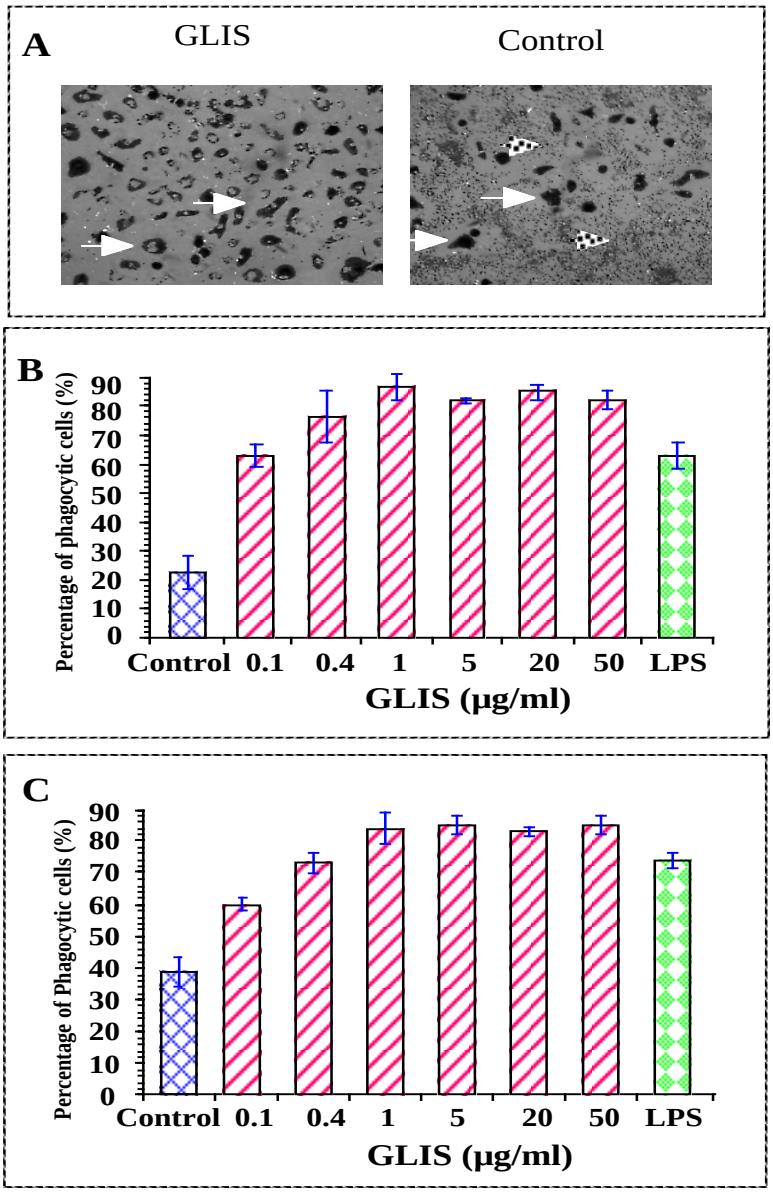


Fig. 5. Phagocytosis of latex beads by macrophages. (A) After BMMs and TBMMs were treated with GLIS in presence of latex beads (latex beads: macrophages = 50:1) for 24 h, morphological changes are observed microscopically. White arrows presented the phagocytic cells, the arrows with points presented the non-phagocytic cells or free latex beads. BMMs (B) and TBMMs (C) were treated with different concentration of GLIS (0.1-50 μg/ml), LPS (1 μg/ml), or 0.9% NaCl as control for 24 h *in vitro*. The suspension of latex beads were washed out, phagocytic cells were counted microscopically. Results present means ± SD of triplicates of one representative experiments.

### 3.1.1.6. Tumour cytotoxicity of macrophages triggered by GLIS

To examine whether GLIS could alter the anti-tumour activities of macrophages, macrophages were stimulated with GLIS in the presence of L929 cells as target cells for 48 h. Fig. 6B shows that the cytolytic percentages of L929 cells were increased dose-dependently in the GLIS-exposed group, while the GLIS itself had no influence on the growth of L929 cells (Fig. 6A).

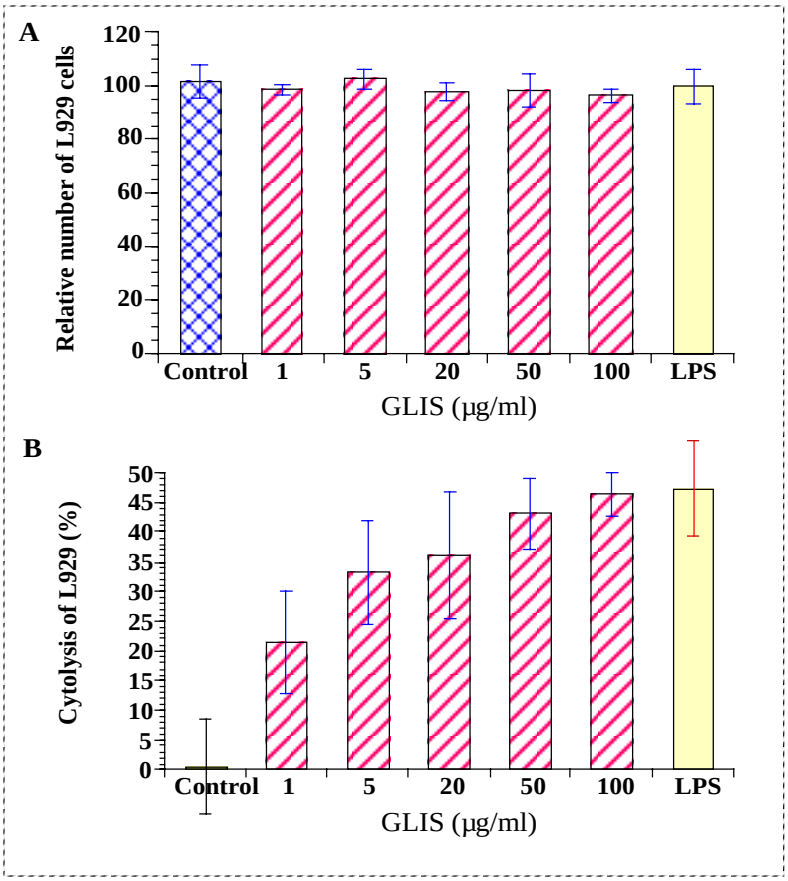


Fig. 6 Tumouricidal activity of GLIS-treated macrophages against L929 cells. (A). L929 cells were treated with various concentrations of GLIS (1-100 μg/ml) or LPS (1 μg/ml) for 48 h. (B) Macrophages were treated with various concentrations of GLIS in the presence of L929 cells, the cytotoxicity was determined after 48 h. Results present means ± SD of triplicates of one representative experiments.

## 3.1.2. Activation and stimulation of B cells by GLIS

### 3.1.2.1. Proliferation of B cells stimulated by GLIS

In the previous work, it was shown that GLIS stimulated the proliferation of lymphocytes, and the percentage of B cell was increased significantly after stimulation by GLIS. But it was still

unclear whether GLIS could stimulate B cells directly. In order to clarify this, B cells were isolated from mouse spleen lymphocytes using CD19 MicroBeads and MiniMACS column. After purification, the percentages of CD19-positive B cells was more than 95% as detected by flow cytometry (Fig. 7A). The remaining cells were non-B cells, containing fewer than 5% CD19 positive cells (B cells), but around 80% CD3 positive cells (T cells). The cell viability was greater than 95%, as determined by trypan blue exclusion.

As shown in Figs. 7B and 7C, the proliferation rate of B cells increased significantly in a dose-dependent manner, while the proliferation rate of non-B cells was not changed by GLIS. The action of GLIS was then compared with other lymphocyte mitogens, such as LPS or PHA. The results (Figs. 7B and C) show that GLIS selectively activates B cells, but not T cells. In addition, at high concentrations (200 μg/ml), the effect of GLIS was dramatically higher than that of 50 μg/ml LPS.

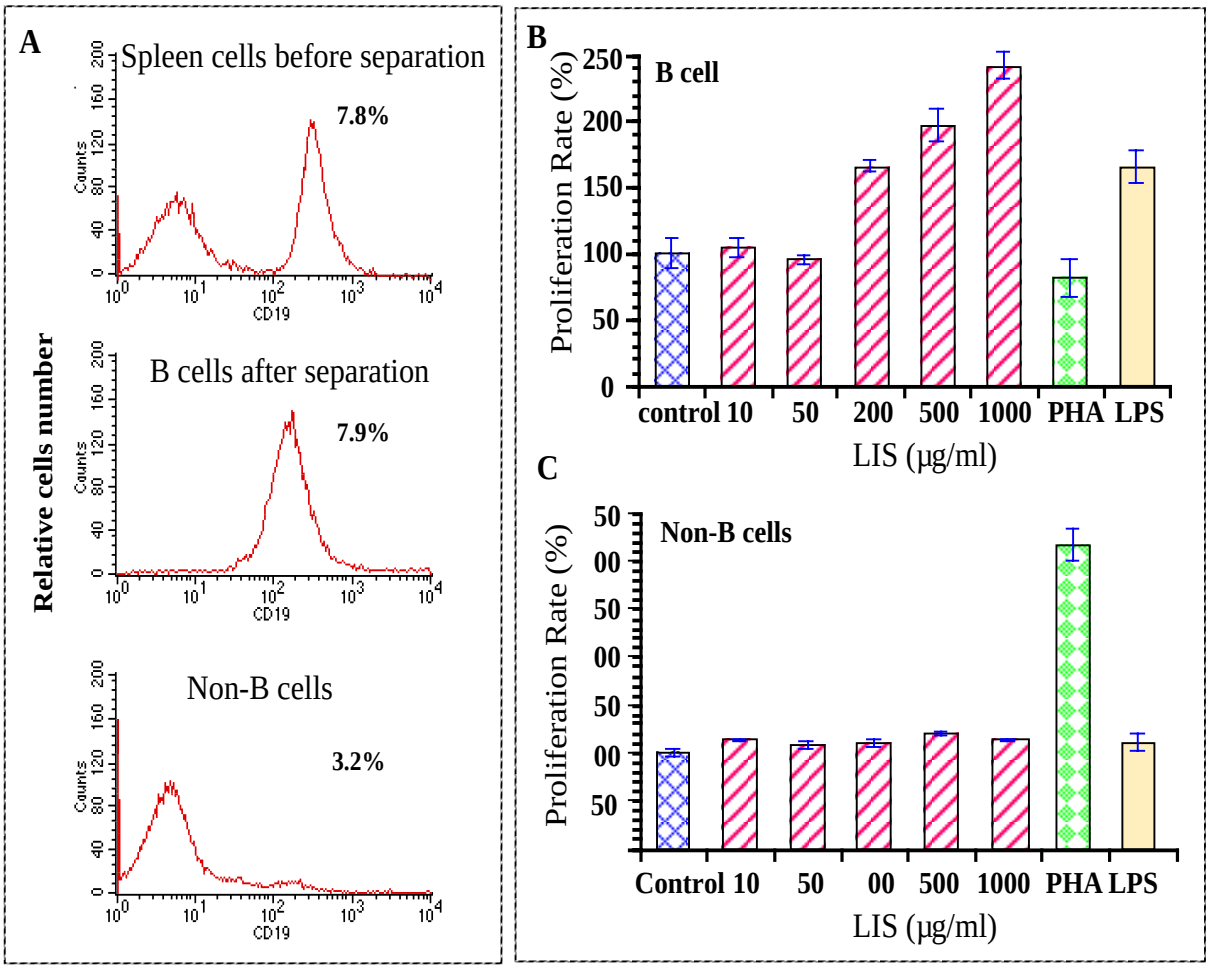


Fig. 7. Proliferation of B cells and non-B cells after stimulation by GLIS. (A) B cells were isolated from MSLs using MACS CD19 MicroBeads and MiniMACS with positive selection column. The purified B cells (B) or non-B cells (C) were treated with different concentrations of GLIS (10-1000 μg/ml), LPS (50 μg/ml), PHA (6 μg/ml) or 0.9% NaCl as control. After stimulation for 72 h, proliferation rate are measured by Alamar Blue Assay. Results present means ± SD of triplicates of one representative experiments.

### 3.1.2.2. Analysis of activation and proliferation of B cells stimulated by GLIS

In order to further confirm that B cells were directly stimulated by GLIS, the expression of CD25 and CD71 on the cell surface was analysed. The results show that the percentages of CD25 and CD71 positive B cells were increased significantly (Fig. 8A), while the percentage of $CD3^+/CD71^+$ cells or $CD3^+/CD25^+$ of non-B cells did not change after stimulation by GLIS (Fig. 8B). Like B cell mitogen LPS, but not the T cell mitogen PHA, GLIS stimulated B cells but not non-B cells to express CD25 and CD71. The results confirmed that GLIS could stimulate B cells directly like LPS.

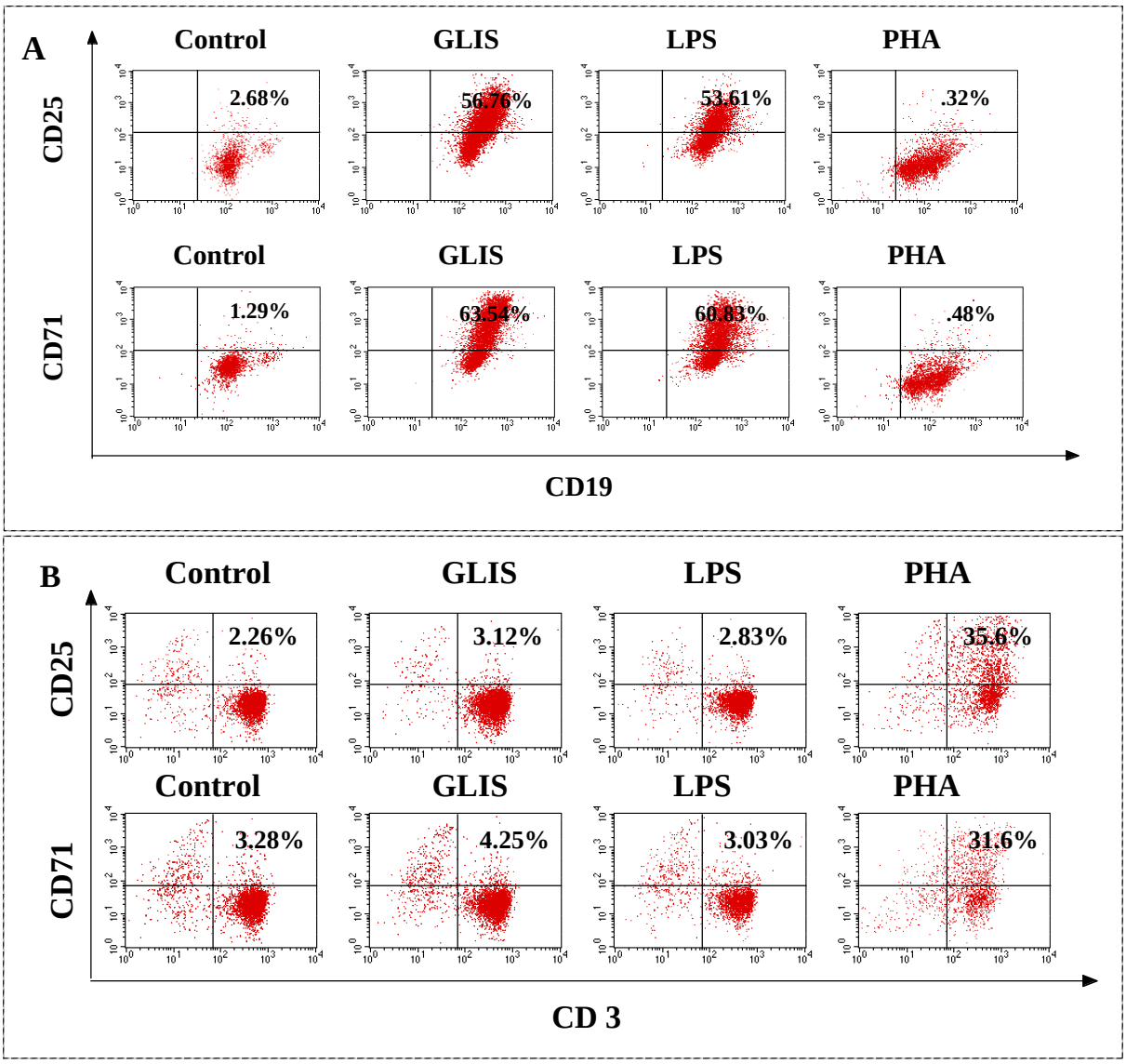


Fig. 8. Flow cytometric analysis of the expression of CD25 and CD71 on B cells or non-B cells stimulated by GLIS. B cells and non-B cells were treated with GLIS 500 μg/ml, LPS 50 μg/ml, PHA (6 μg/ml) or 0.9% NaCl as control for 48 h. B Cells were stained with anti-mouse CD19-FITC/CD25-PE or CD19-FITC/CD71-PE (A), non-B cells were stained with anti-mouse CD3-FITC / CD71-PE or CD3-FITC / CD25-PE (B).

### 3.1.2.3. Secretion of immunoglobulin by MSLs and B cells after stimulation with GLIS

#### 3.1.2.3.1. Secretion of IgM and IgG by MSLs after stimulation by GLIS

The effects of GLIS on B cells were further examined by determining the increased concentration of IgM and IgG antibody in the medium. Fig. 9A shows that MSLs secrete tremendous amounts of IgM after stimulation by GLIS. Furthermore, secretion of IgM was increased daily until day 6. MSLs also secreted low concentrations of IgG as shown in Fig. 9B. The effect of GLIS on the secretion of immunoglobulin was comparable to that of LPS.

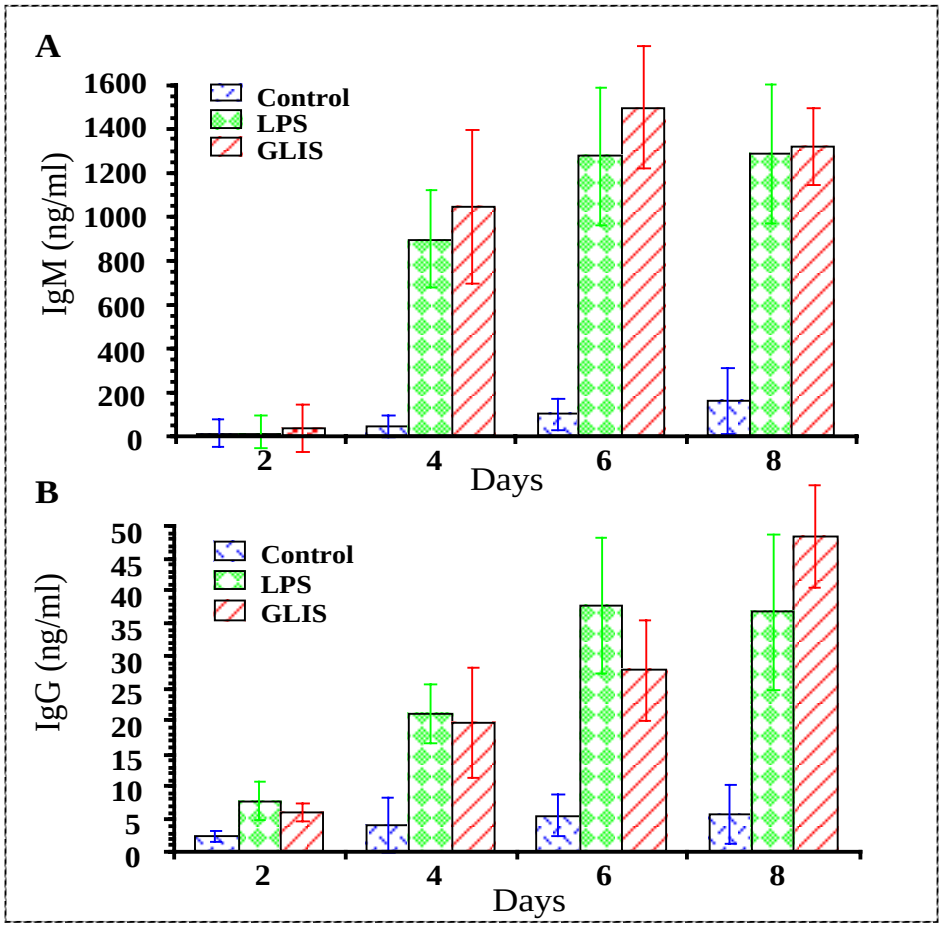


Fig. 9. Secretion of IgM and IgG by MSLs after stimulation by GLIS. MSLs were incubated with 500 µg/ml of GLIS, 50 µg/ml of LPS or 0.9% NaCl as control. At the times indicated, the aliquots of supernatants were taken for determination of the concentrations of IgM and IgG by ELISA. Results present means ± SD of 3 different experiments.

#### 3.1.2.3.2. Secretion of IgM and IgG by B cells after stimulation by GLIS

B cells could be directly stimulated by GLIS as mentioned above. The secretion of IgM and IgG by B cells was also analysed by ELISA. Fig. 10 shows that purified B cells could secrete significant amounts of IgM after stimulation by GLIS. With respect to the response of MSLs, the relative amount of IgM secreted by B cells was lower than that by MSLs (320 ng/ml vs.

1400 ng/ml) (Fig. 10A vs. Fig. 9A). The amount of IgG secreted by B cells was also 3-4 times lower than that secreted by MSLs (11 ng/ml vs. 35 ng/ml) (Fig. 10B vs. Fig. 9B). In comparison to GLIS, the secretion of IgM and IgG of B cells was also lower than that of MSLs after stimulation by LPS (540 ng/ml vs. 1400 ng/ml (18 ng/ml vs. 45 ng/ml). These results suggest that the response of purified B cells to both GLIS and LPS is very low in the absence of accessory cells, whereas with the help of other cells, the response of B cells to both GLIS and LPS is increased dramatically.

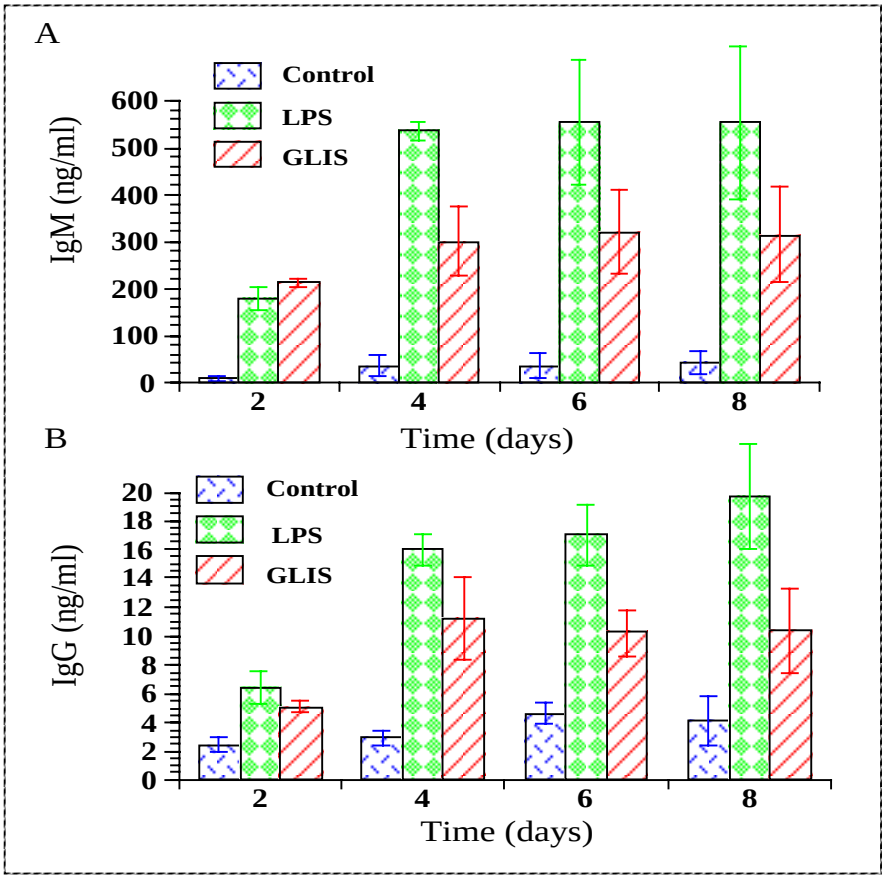


Fig. 10. Secretion of IgM and IgG by B cells after stimulation by GLIS. Isolated B cells were incubated with 500 µg/ml of GLIS, 50 µg/ml of LPS, 0.9% NaCl as control. At the indicated times, aliquots of supernatants were taken for determination of the concentration of IgM and IgG by ELISA. Results present means ± SD of 3 different experiments.

## 3.1.3. Interaction of B cells and macrophages after stimulation with GLIS

### 3.1.3.1. Increase of survival of B cells in presence of macrophages after stimulation with GLIS

B cells could be directly stimulated to activation, proliferation and secretion of immunoglobulin by GLIS. However, the amount of IgM and IgG secreted by B cells was 2-3

times lower than that by MSLs. This suggests that some other cells stimulate B cells to secrete IgM or IgG. GLIS has no obvious effect on the proliferation and activation of T cells, but GLIS can activate macrophages to secrete cytokines and NO, and can increase the capacities of phagocytosis.

In the presence of macrophages, B cell survival was increased after stimulation by GLIS. The percentage of dead B cells was measured by FACS analysis with propidium iodide staining. Without GLIS stimulation, B cells alone could hardly survive 4 days in culture medium, but co-incubation with macrophages increased the survival rate of B cells to 9%. When B cells were stimulated by GLIS, almost 95% of the cells were dead by the fourth day, whereas 51% of the B cells were still viable in the presence of macrophages. This finding suggests that macrophages could increase the survival of B cells in the presence of GLIS (Fig. 11).

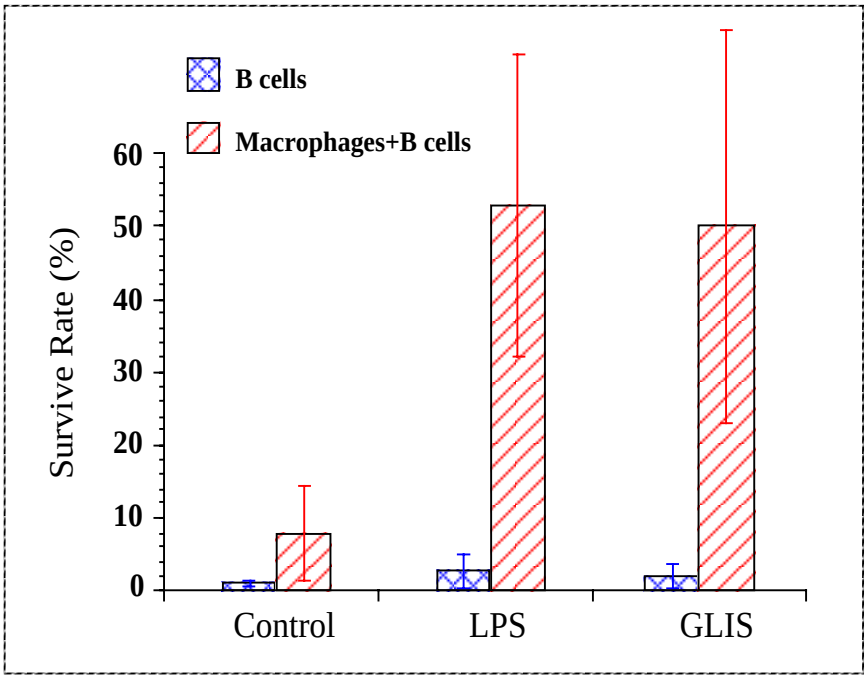


Fig. 11. Viabilty of B cells by co-incubation with macrophages. B cells with or without 0.5% macrophages were stimulated with 500 µg/ml GLIS, 50 µg/ml LPS or 0.9% NaCl as control for 4 days in culture. Percentages of the dead B cells were measured by FACS analysis with propidium iodide staining. Results present means ± SD of 3 different experiments.

### 3.1.3.2. Secretion of IgM by B cells in presence of macrophages after stimulation with GLIS

Survival of B cells was increased by macrophages treated by GLIS. It remained to be determined whether the macrophages influenced B cells to increase their IgM secretion. The capacity of IgM secretion by B cells was measured after stimulation with GLIS in the

presence of 0.5% macrophages. The secretion of IgM was increased two times in the presence of macrophages stimulated by GLIS (Fig. 12).

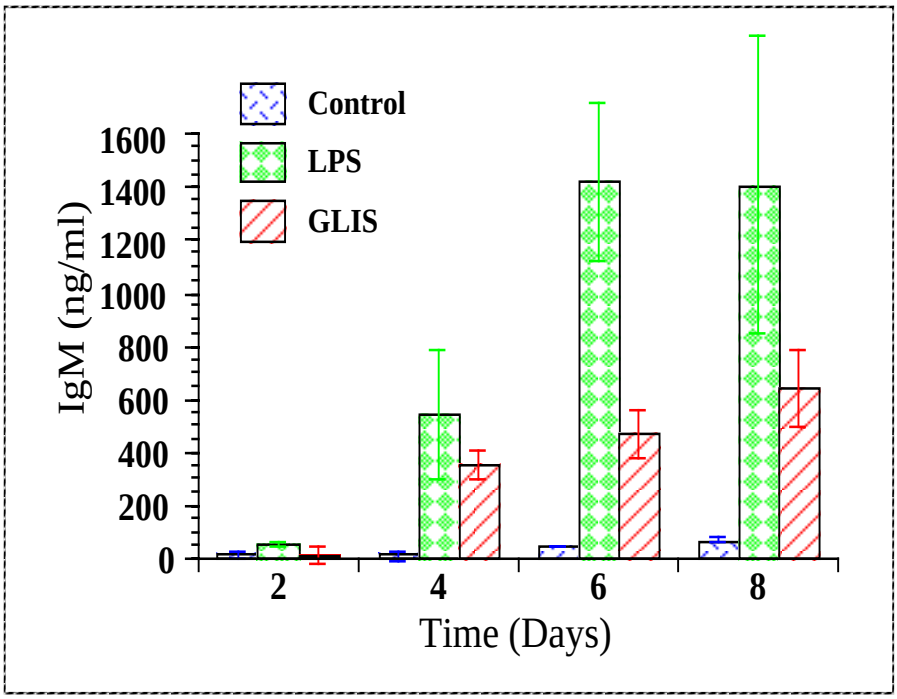


Fig. 12. Secretion of IgM by B cells co-cultured with macrophages. B cells co-cultured with $10^4$ macrophages were stimulated with 500 mg/ml GLIS. 50 µg/ml LPS or 0.9% NaCl as control for different time. At the indicated times, aliquots of supernatant were taken for determination of the concentration of IgM by ELISA. Results present means ± SD of 3 different experiments.

### 3.1.3.3. Effect of IL-6 or supernatants of macrophages on the B cell

Macrophages could significantly increase the IgM secretion of B cells after stimulation with GLIS. It remains to be determined whether these B cells interact directly with macrophages or through various substances secreted by macrophages such as cytokines.

Furthermore, it was found that IL-6 and the supernatant of macrophages could not prolong the survival of the B cells as do macrophages in the presence of GLIS. IL-6 could stimulate the B cells to secrete IgM, but could not increase the IgM secretion of B cells in the presence of GLIS or LPS. The supernatants of macrophages could not stimulate B cells to secrete IgM. But in presence of the supernatant of macrophages which had been stimulated with GLIS, IgM secretion of B cells stimulated by GLIS was slightly enhanced (Fig. 13B). The results suggest that the increase of B cell survival and IgM secretion is primarily influenced by direct interaction with macrophages.

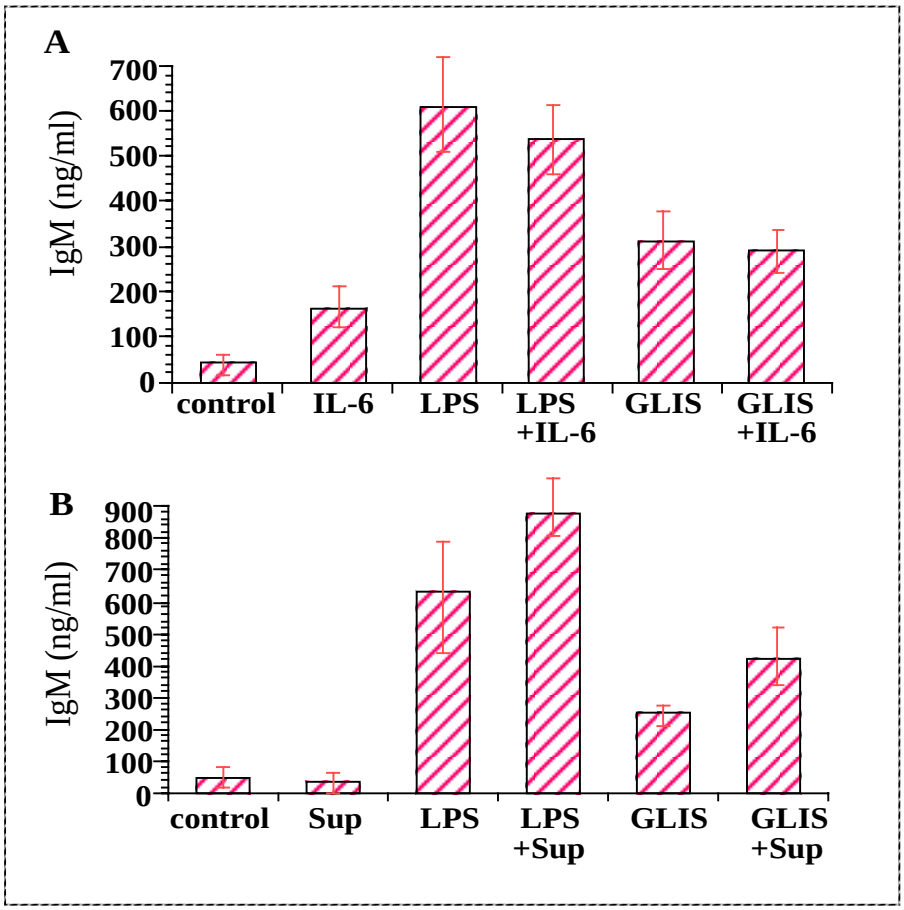


Fig. 13. Secretion of IgM by purified B cells stimulated wtih GLIS in presence of IL-6 or the supernatant of macrophages. (A) B cells were stimulated by 500 µg/ml GLIS, 50 µg/ml LPS or 0.9 NaCl as control for 8 days in presence or absence of IL-6, the supernatant was used for detection of the IgM. (B) B cells were stimulated with 500 µg/ml GLIS, 50 µg/ml LPS or 0.9 NaCl as control for 8 days in presence or absence of the supernatant of macrophages for 8 days, supernatant were used for detection of IgM. Results present means ± SD of 3 different experiments.

## 3.1.4. B cells from tumour-bearing mice (TMSBs) stimulated by GLIS

### 3.1.4.1. Proliferation and activation of TMSBs after stimulation by GLIS

As a prelude to the characterisation of GLIS in tumour bearing mice, the effect of progressive tumour growth on spleen weight and spleen cellularity was analysed. After the mice were injected with tumour cells, their spleens were removed 3 weeks later and the spleen cells were characterised by flow cytometry. Compared with that of normal mice, the spleens of tumour-bearing mice were larger, and the number of the splenocytes of tumour bearing mice was 4-5 times greater compared to normal mice. The percentage of CD19 positive B cells in the

splenocytes of tumour-bearing mice was only 1/2 as that of normal mice, and the percentage of CD3 positive T cells was only 1/3 as that of normal mice (Table. 1).

| | Tumour mice | Normal mice |
|---|---|---|
| Weight | 0.39 ± 0.021 | 0.12 ± 0.008 |
| Cell number | $2.87 \pm 0.53 \times 10^8$ | $5.2 \pm 0.32 \times 10^7$ |
| CD3+ | 12.44 ± 0.3 (%) | 32.2 ± 2.1 (%) |
| CD19+ | 22.71 ± 3.1 (%) | 47.8 ± 6.3 (%) |

Table 1. Comparison of normal and tumour mice spleen

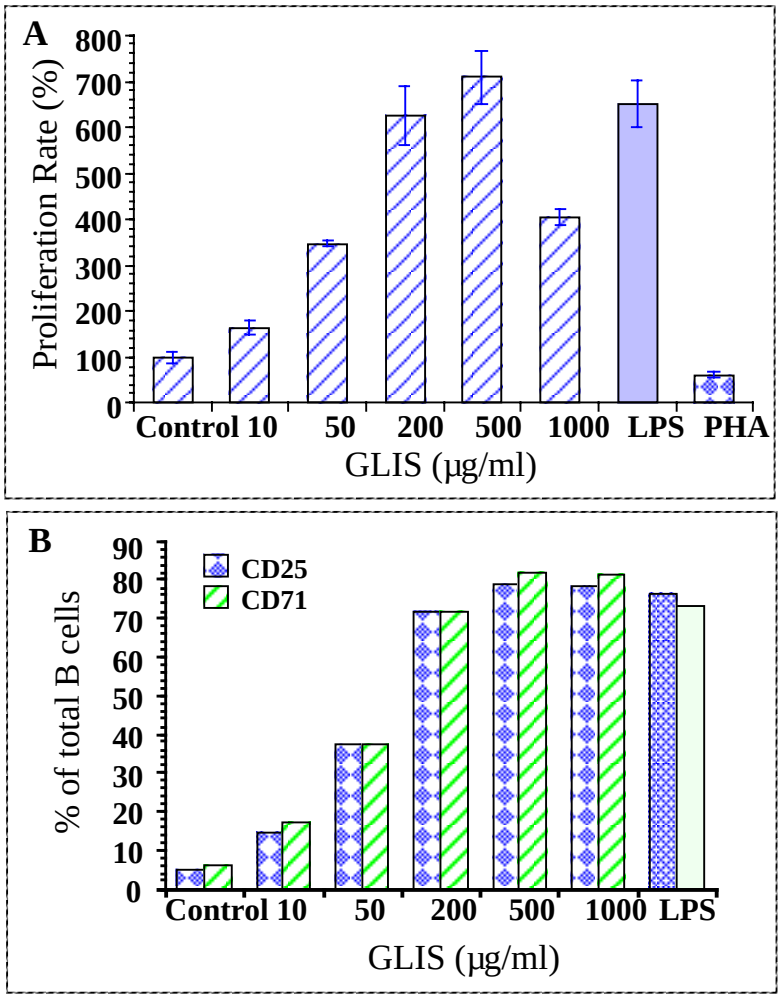


Fig.14 . Proliferation and activation of B cells from tumour-bearing mice. The B cells were purified from TMSLs by positive selection column and stimulated by different concentration of GLIS (10-1000 μg/ml), LPS (50 μg/ml), PHA(6 μg/ml) or 0.9% NaCl as control for 72 h. Proliferation was measured using Alamar Blue Assay (A). Results present mean ± SD of 3 different experiments. The percentage of CD25 or CD71 positive cells was detected by flow cytometric analysis (B).

It is known that immune response is reduced in a tumour-bearing host (Chaux, 1995). Previous studies have shown that the proliferation rate of mouse spleen lymphocytes from tumour-bearing mice was higher than that from normal mice (Zhang, 2000). B cells isolated from tumour-bearing mice were stimulated with GLIS. The proliferation of B cells from TMSLs increased significantly after stimulation by GLIS or LPS (Fig. 14A). PHA, which is mitogenic to T cells, showed a slight inhibition on the proliferation of purified B cells from TMSLs at 6 μg/ml. FACS analysis also showed that GLIS-stimulation of B cells led to an increase in the proportion of CD71 and CD25 positive cells (Fig. 14B). The percentages of CD25 and CD71 were 78% and 82%, respectively, in tumour bearing mice, but 56% and 63%, respectively, in normal mice. These results suggest that B cells isolated from TMSLs could also be activated directly by GLIS and in a more sensitive manner than MSBs.

### 3.1.4.2. Secretion of IgM by TMSLs and TMBS after stimulation by GLIS

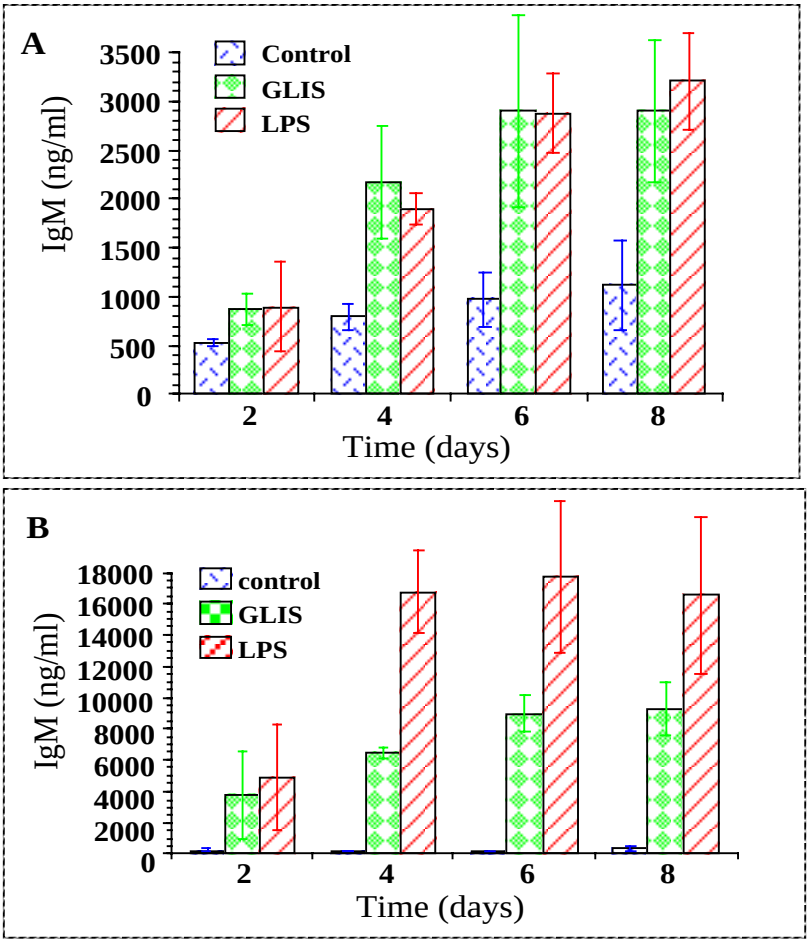


Fig.15. Secretion of IgM by BMMs and TBMMs after stimulated by GLIS. TMSLs (A) or TBMMs (B) were incubated with 500 μg/ml of GLIS, 50 μg/ml of LPS or 0.9% NaCl as control. At the times indicated, the aliquots of supernatants were taken for determination of the concentration of IgM by ELISA. Results present means ± SD of 3 different experiments.

TMSLs secreted significant amounts of IgM after stimulation by GLIS (Fig 15A). The amount of IgM secreted by TMSLs was about five times that by MSLs (Fig. 9). B cells from TMSLs secreted 9 µg/ml IgM after being stimulated by GLIS (Fig. 15B). Compared to MSBs (Fig. 10), TMSBs produced more than ten times IgM (Fig. 15B) than MSBs, suggesting that TMSLs and TMSBs were more sensitive to GLIS than MSLs and MSBs with respect to the secretion of IgM.

### 3.1.5. IgM secretion of normal mice stimulated by GLIS *in vivo*

In order to evaluate the response of mice to GLIS *in vivo*, mice serum IgM secretion was measured after being injected with GLIS. GLIS induced a significant increase of IgM from day 6 to day 25 in comparison to the control (Fig. 16).

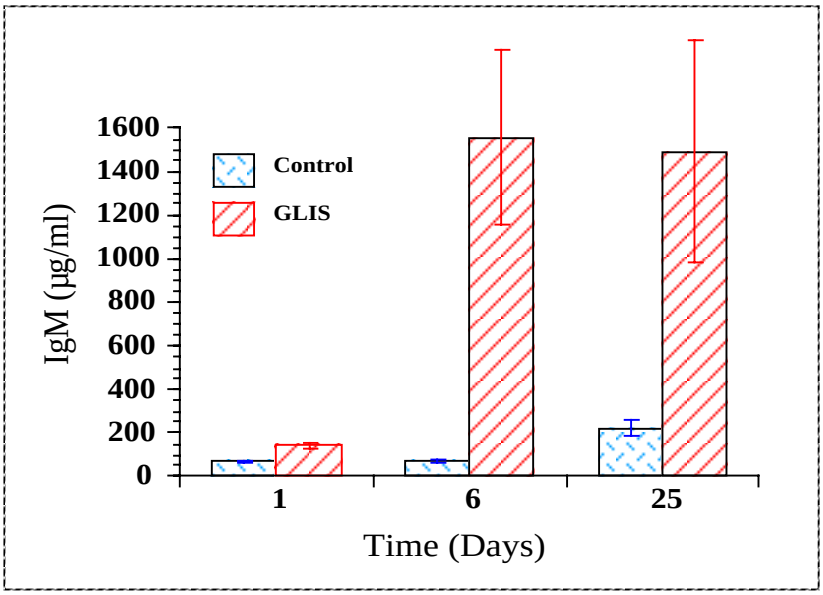


Fig. 16. Secretion of IgM in serum after injection to mice with GLIS *in vivo*. The mice were injected with GLIS or PBS per 3 days, 5 times. The serum at day 0, 6 and 25 were taken for determination of the concentration of IgM by ELISA. Results present means ± SD of 3 different experiments.

### 3.1.6. Characterisation of the active fraction GLIS

#### 3.1.6.1. Comparison of the properties of GLIS with LPS

Since GLIS was found to activate B cells and macrophages in a manner similar to LPS, the modes of action of GLIS and LPS were compared. Polymyxin B, a selective inhibitor of LPS, is known to inhibit the LPS-induced activation of macrophages by binding the lipid A moiety of LPS. Polymyxin B abolished LPS-induced proliferation of MSLs, and the activation and NO production of macrophages as well, whereas it did not inhibit GLIS-induced MSLs proliferation, nor the activation and NO production of macrophages (Figs. 17A, B and C).

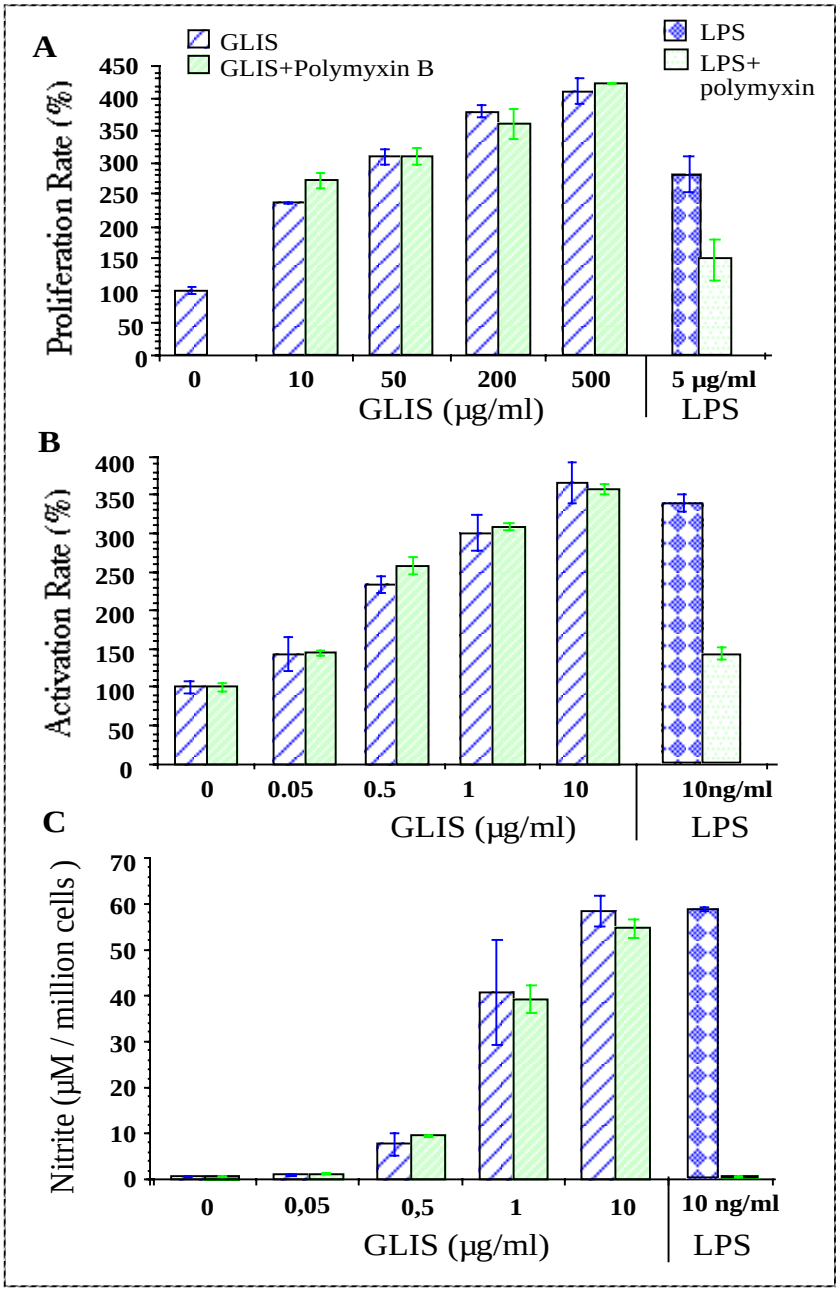


Fig. 17. Effect of Polymyxin B on LPS and GLIS-activation of MSLs or macrophages. MSLs (A) or macrophages (B) were stimulated 72 h with GLIS or LPS which were preincubated with or without polymyxin B (10 µg/ml), the proliferation or activation rate were assayed with Alamar Blue method. (C) Macrophages were stimulated 24 h with GLIS or LPS which were preincubated with or without polymyxin B (10 µg/ml), the supernatants were harvested and assayed for nitrite. Results present means ± SD of triplicates of one representative experiments.

We also used MSLs and BMMs from C3H/HeJ mice, which were low responders to LPS, in order to check the difference between LPS and GLIS. GLIS significantly stimulated the

proliferation of MSLs and the activation of macrophages, and enhanced the NO production of macrophages from both C3H/HeJ and Balb$^c$ mice (Figs.18A, B and C). On the other hand, LPS was able to stimulate the proliferation of MSLs activation and enhance the NO production of macrophages from Babl$^c$ mice but not from C3H/HeJ mice. The results suggest that the activity of GLIS is not due to the contamination with LPS.

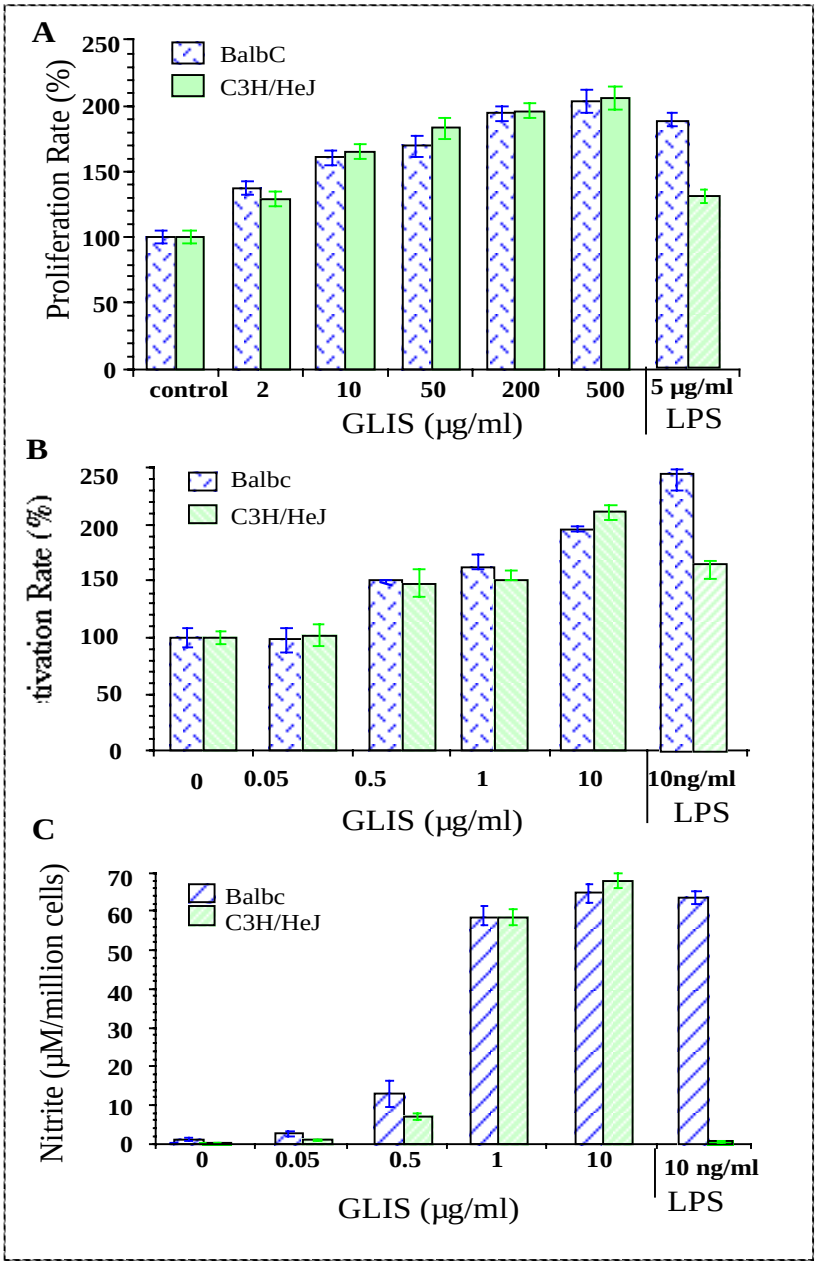


Fig. 18 Response of LPS or GLIS to macrophages from Babl$^c$ mice or C3H/HeJ mice. MSLs (A) or Macrophages (B) from Babl$^c$ mice or C3H/HeJ were treated with GLIS or LPS for 72 h, the proliferation or activation rate were assayed with the Alamar Blue method. (C) Macrophages were stimulated 24 h with GLIS or LPS, the supernatants were harvested and assayed for nitrite. Results present means ± SD of triplicates of one representative experiments.

### 3.1.6.2. Structural analysis of the functional compound of GLIS

Previous work has shown that GLIS is a proteoglycan with a carbohydrate:protein ratio of 11.5:1. In this work the functional structure of GLIS was analysed. The protein or peptide part of GLIS was removed by digestion with Pronase E. The carbohydrate part of GLIS was destroyed by $NaIO_4$. Fig. 19 shows the MSLs proliferation rate after stimulation by GLIS, which was pretreated with Pronase E or $NaIO_4$. It was found that the activity of GLIS remained unchanged after treatment with Pronase E, while the activity of GLIS was almost lost after treatment with $NaIO_4$. These results suggest that the activity of GLIS is attributed to its polysaccharide constituent.

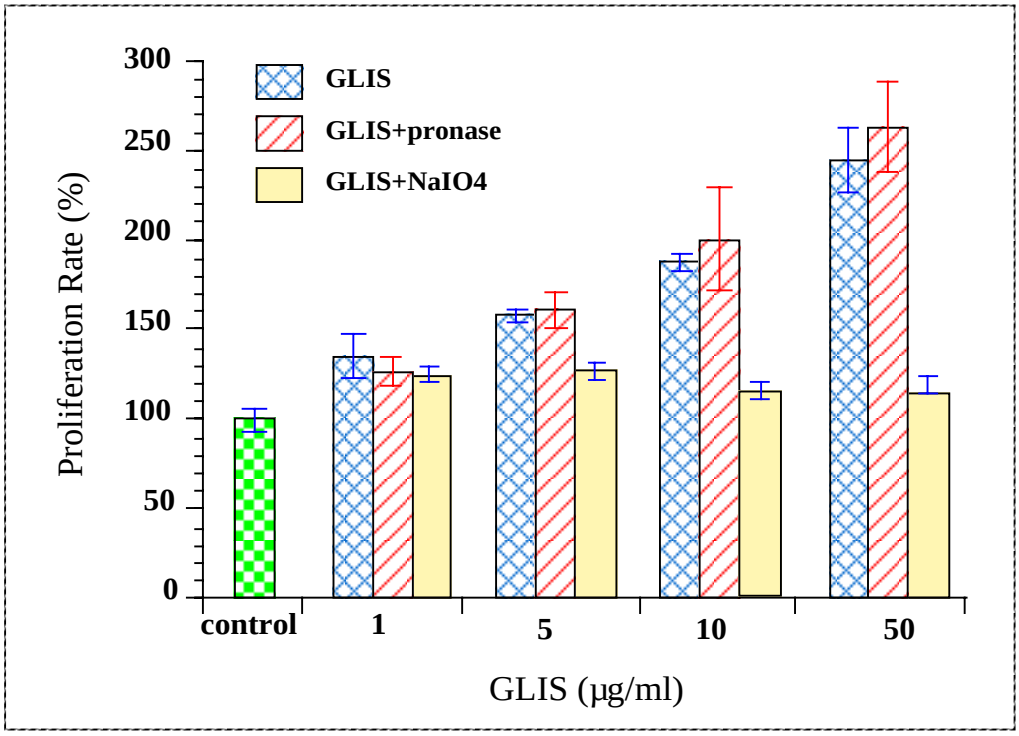


Fig. 19. Proliferation of MSLs after stimulation by GLIS pretreated with Pronase E or $NaIO_4$. GLIS was treated with 0.5 mg/ml Pronase E for 48 h or NaIO4 for 4 h. The sample were used for stimulation of MSLs for 72 h with the concentrations indicated. The proliferation rates were measured by Alamar Blue Assay. Results present means ± SD of triplicates of one representative experiments.

### 3.1.6.3. Reduction of GLIS activity after digestion of GLIS with β-1,3-glucanase

Because glucose is one of the main components of GLIS, a relationship of the biological activity to the type of glycosidic bindings must be demonstrated. GLIS was digested by β-1,3-glucanase before the biological testing. The results (Fig. 20) showed that the macrophage activation rate was abolished by GLIS digested by β-1,3-glucanase. This observation suggests that β-glucosyl bindings of GLIS are important for macrophage activation.

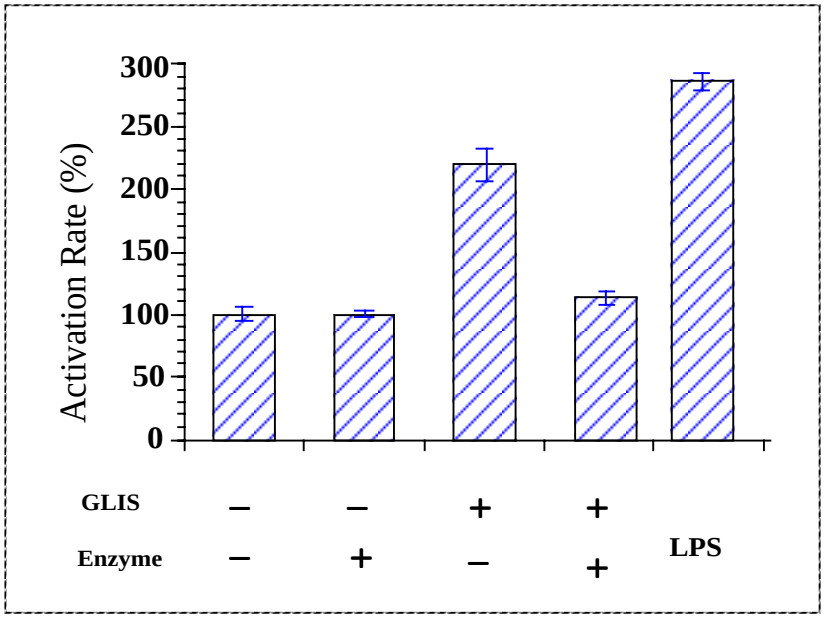


Fig. 20. Activation of macrophages by GLIS predigested with β-1,3-glucanase. GLIS was treated with β-1,3-glucanase for 24 h at 25°C, after heated with 100°C for 10 min. The sample (1 μg/ml) was used to stimulate macrophages for 72 h. The activation rate of macrophages was detected by Almar Blue Assay. Results present means ± SD of triplicates of one representative experiments.

### 3.1.6.4. Purification and determination of the molecular weight of GLIS using gel-filtration HPLC

GLIS was checked by HPLC using a GF-450 coupled to GF-250 gel-filtration column (Fig. 21A). One main peak at 26.3 min and another mini peak at about 17 min were found by UV detection. The eluates were collected according to the elution time and the concentrations of carbohydrate in every fraction were measured by dot-blot using a Glycan detection kit (Fig, 21B). It was found that fractions 16-18 contained carbohydrate, with the highest concentration in fraction 17. According to the dot-blot, the integrated density units of each fraction showed that the fraction was a single peak. At the same time, all the fractions were examined for bioassay (Fig. 21C) showing that fractions 16-18 were able to stimulate macrophages. The activities paralleled the concentrations of carbohydrates. This suggests that the fraction containing carbohydrate is active, rather than the 16.8 kDa fraction. The molecular weight of the fraction was estimated by comparing the retention time of the tested sample to the standard. It is estimated as ca. 2000 kDa.

After purification by HPLC, the carbohydrate containing fraction 17 was purified without the 16.8 kDa peak. After hydrolysis with trifluoroacetic acid (TFA), the molar ratio of different monosaccharides was determined through high-pH anion-exchange chromatography of the Dionex equipment. The active fraction consisted of 7 different monosacchrides (Table 2).

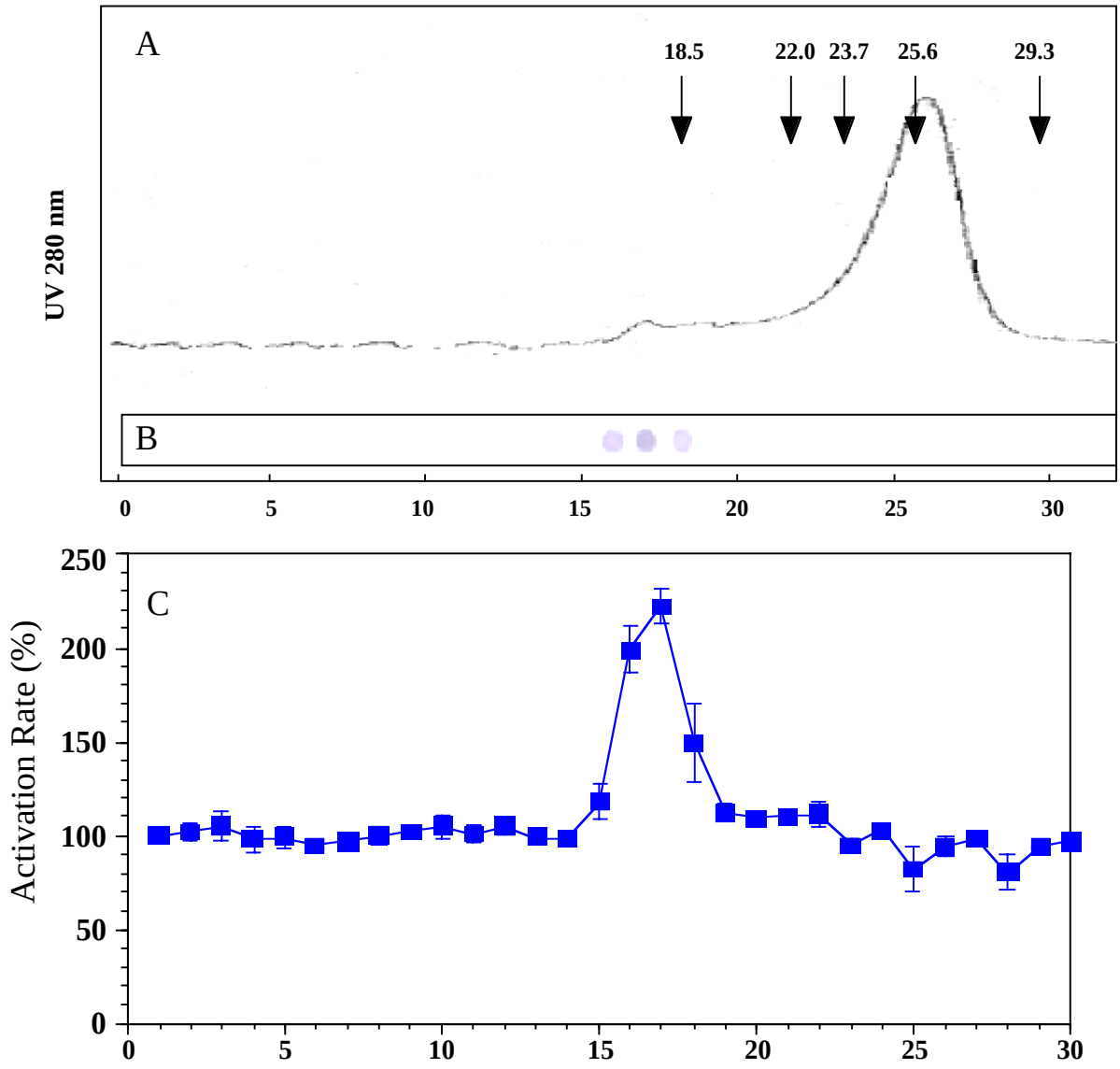


Fig. 21. Enrichment of the active fraction of GLIS using gel-filtration HPLC. (A) The elution profile of HPLC of standard and GLIS on a GF-450 coupled to GF-250 gel filtration column. The retention time/Mr of standards are 18.5/670k, 22.0/158k, 23.7/44k, 25.6/17k and 29.3/1.35k, respectively. (B) The concentration of carbohydrates in every fraction from HPLC was measured by dot-blot analysis using Glycan Detection Kit. (C) Every fraction was used to stimulate macrophages, the activation rate of macrophages was measured using Alamar Blue Assay. Results present means ± SD of triplicates of one representative experiments.

| Fucose | Ara | GalNH2 | Gal | GlcNH2 | Glu | Man | Xyl |
|---|---|---|---|---|---|---|---|
| 1.0 | 4.1 | 0.3 | 4.9 | 0.4 | 7.2 | 3.6 | 1.2 |

Table. 2 The molar ratio of different monosaccharides in the active fraction. Fuc: fucose; GalNH2: galactosamine; GlcNH2: glucosamine; Ara: arabinose; Gal: galactose, Glu: glucose; Man: mannose; Xyl: xylose.

## 3.1.7. Investigation of the mechanism of action of the active fraction GLIS

### 3.1.7.1. Binding of FITC-GLIS to macrophages

The above results indicate that GLIS can activate macrophages. The mechanism of activation is still unclear. It was first tested whether GLIS could bind to macrophages. GLIS was conjugated with fluorescent isothiocyanate (FITC). Flow cytometry was employed to investigate the binding of FITC-labelled GLIS to bone marrow-derived macrophages and macrophages cell lines U937 and J774. It was found that FITC-labelled GLIS could stain U937, J774 cell lines and macrophages (Fig. 22). These results suggest that GLIS could bind to macrophage.

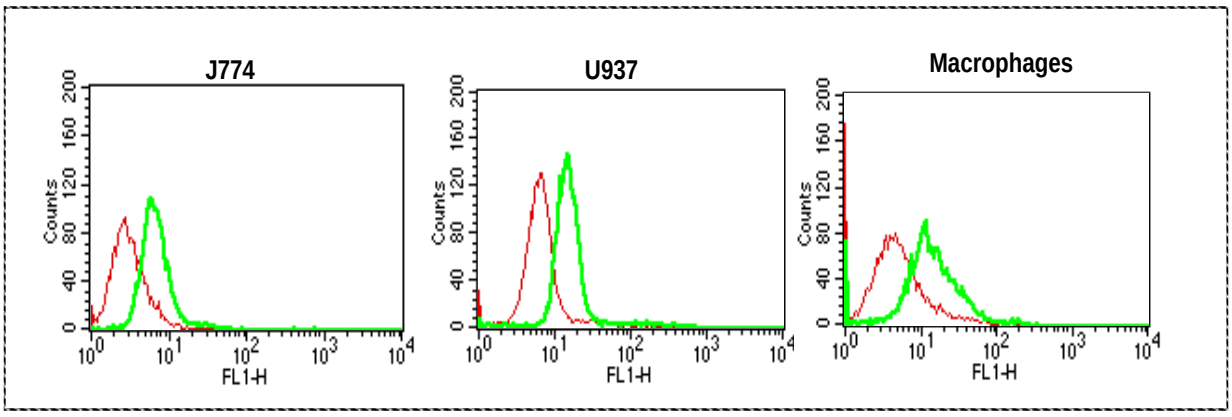


Fig. 22. FACS analysis of binding of GLIS-FITC to macrophages and macrophages cell line. BMMs, J774 or U937 cells were incubated for 1 h at 37 °C with 1 µg/ml GLIS-FITC in 100 µl DMEM medium. The cells were detected by flow cytometry.

### 3.1.7.2. Inhibition of soluble β-glucan-, mannose receptor- antagonist and anti-CD14 antibody on the activity of GLIS

Preincubation of macrophages with laminarin, a soluble carbohydrate antagonist of the macrophage β-glucan receptor, reduced significantly macrophage after GLIS treatment. After treatment with laminarin, the nitrite production of macrophages stimulated by GLIS was reduced by 30% compared with treatment with a saline buffer only. Preincubation of macrophages in the presence of α-mannan, a soluble antagonist of the macrophage mannose receptor, also significantly reduced macrophage nitrite production following treatment with GLIS. Following treatment with α-mannan, the nitrite production of macrophages was reduced by 45% compared with treatment with a saline buffer only (Fig. 23). Treatment of macrophages with anti-CD14 Ab reduced about 60% the GLIS-induced nitrite production. These results suggest that the effect of GLIS on macrophages was related to the β-glucan receptor, the mannose receptor and the membrane protein CD14.

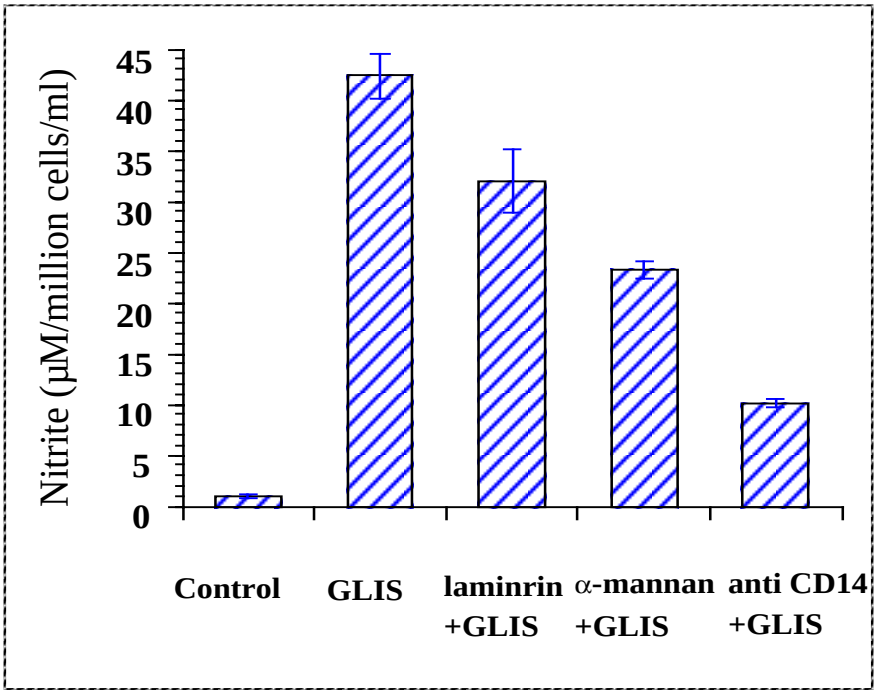


Fig. 23. The influence of GLIS with soluble β-glucan, mannose antagonist and anti-CD14 Ab on nitrite release of macrophages in response to GLIS. Preincubation of macrophages with soluble β-glucan receptor antagonist laminrin (0.5 μg/ml), mannose antagonist α-mannan (0.5 μg/ml) or anti-CD14 Ab (5 μg/ml) for 45 min followed by treatment with GLIS for 24 h. Culture supernatant were harvested and assayed for nitrite. Results present means ± SD of triplicates of one representative experiments.

## 3.2. Induction of tumour cells apoptosis by compounds from *Polygonum cuspidatum*

### 3.2.1. Inhibition of proliferation and induction of tumour cells apoptosis by *Polygonum cuspidatum*

#### 3.2.1.1 Inhibition of proliferation of SW620 cells by fractions and subfractions of *Polygonum cuspidatum*

The crude extract HZ from the plant *Polygonum cuspidatum* demonstrated significant inhibition of the proliferation of tumour cells (Li, 2000). In order to find out the active components in the crude extract, HZ was fractionated and the fractions were tested with respect to their antitumour activity. The purification strategy was comprised of a multi-step procedure including extraction, pre-purification and chromatographic steps.

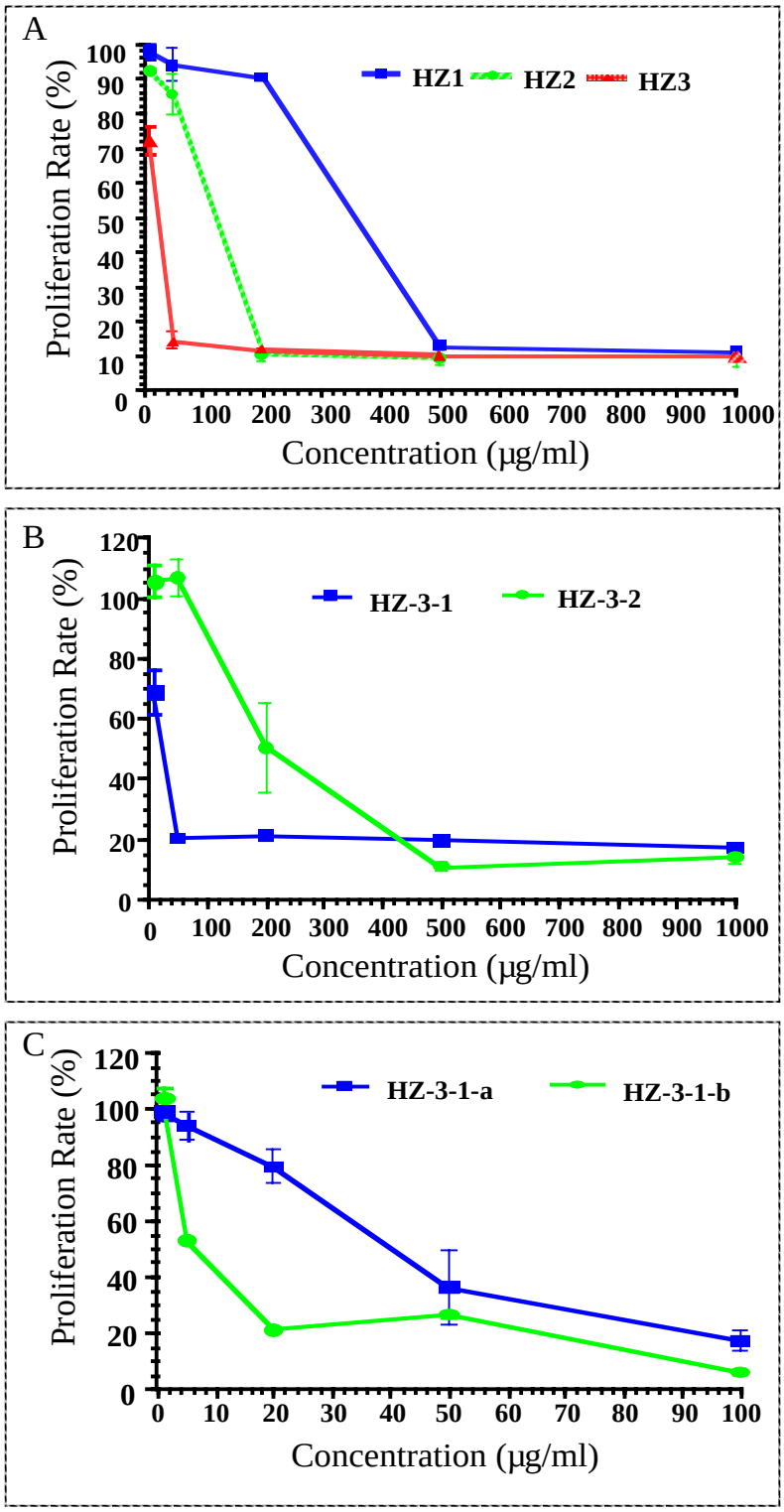


Fig. 24. Inhibition of proliferation of SW620 cells by the fractions and subfractions of HZ. After SW620 cells were treated by A: fractions of HZ, B: Fractions of HZ-3, C: Fractions of HZ-3-1 at different concentration for 72 h, the proliferation rate were measured by Alamar Blue Assay. Results present means ± SD of triplicates of one representative experiments.

HZ was fractionated to HZ-1, HZ-2 and HZ-3. The IC50 (inhibitory concentration, 50%) of these three fractions were 360 µg/ml, 120 µg/ml and 30 µg/ml, respectively (Fig. 24A). The most active fraction, HZ-3, was further divided into two subfractions HZ-3-1 and HZ-3-2 according to their solubility in water; their IC50 were 20 µg/ml and 200 µg/ml, respectively (Fig. 24B). After further purification of HZ-3-1 by HPLC, the two fractions HZ-3-1-a and HZ-3-1-b were achieved. Each showed one peak by HPLC screening. Their IC50s were 42 µg/ml and 5 µg/ml, respectively (Fig. 24C). The results suggest that HZ-3-1-b is the most active fraction in the crude extract of HZ with regard to the inhibition of growth of SW620 cells.

#### 3.2.1.2. Inhibition of proliferation of different tumour cell lines by the active fraction HZ-3-1-b

The anti-proliferation capacity of HZ-3-1-b was further tested using 10 different tumour cell lines. HZ-3-1-b inhibited the proliferation of various kinds of tumour cells in a dose-dependent manner (Fig. 25). It was found that HZ-3-1-b inhibited the proliferation of the tumour cells MCF-7 and LS180, respectively, but only in high concentrations (4-20 µg/ml); low concentrations of HZ-3-1-b (0-2 µg/ml) increased the proliferation of these two tumour cells lines.

#### 3.2.1.3. Identification of apoptosis of SW620 cells induced by HZ-3-1-b

It is known that many carcinostatics act by inducing apoptosis of tumour cells. To determine whether the anti-proliferative effect of HZ-3-1-b was associated with apoptosis, the morphological changes of SW620 cells were examined after treatment with 10 µg/ml HZ-3-1-b for 24 h. Cells exposed to HZ-3-1-b exhibited distinct morphological features of programmed cell death such as shrinkage and apoptotic body *in situ* when checked by light microscopy (Fig. 26A).

To confirm that SW620 cells had undergone apoptosis, the cells were stained with annexin V-FITC conjugate. Annexin V is an anticoagulant protein that preferentially binds to negatively charged phospholipids. During early apoptotic processes, phospholipid asymmetry is disrupted, leading to the exposure of phosphatidylserine to the outer leaf of the cytoplasmic membrane. It is accessible for annexin V binding, so annexin V can be used to detect the apoptotic cells. By fluorescent microscope it was found that part of the cells were labelled by annexin V-FITC (Fig. 26B), suggesting that SW620 cells had undergone apoptosis following HZ-3-1-b treatment..

#### 3.2.1.4. Analysis of DNA fragmentation of SW620 cells after treatment with HZ-3-1-b

In addition to morphological evaluation, induction of apoptosis by HZ-3-1-b was ascertained by measurement of DNA fragmentation. DNA fragmentation is a typical feature of apoptotic cells, occurring as a result of DNA breakdown by endonuclease which become active during the apoptotic process. Propidium iodide (PI) can specifically stain DNA. The whole DNA and its fraction can be distinguished according to the intensity of the fluorescence of DNA stained by PI.

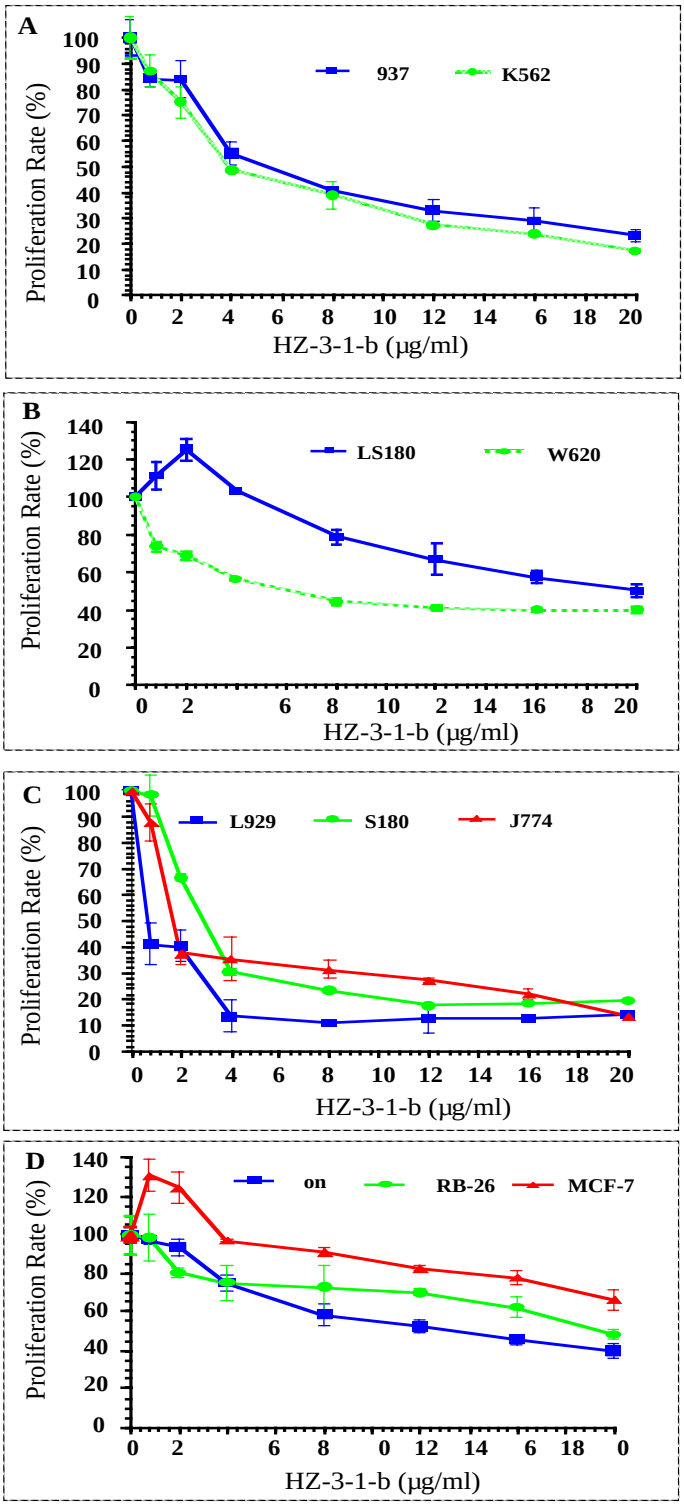


Fig. 25. Inhibition of proliferation of different tumour cell lines by HZ-3-1-b. After A: U937, K562 cells, B: SW620, LS180 cells, C: L929, S180, J774 cells, D: Bon, HRB-26 cells, MCF-7 cells, were treated with different concentration of HZ-3-1-b for 72 h, proliferation rate were measure by Alamar Blue Assay. Results present means ± SD of triplicates of one representative experiments.

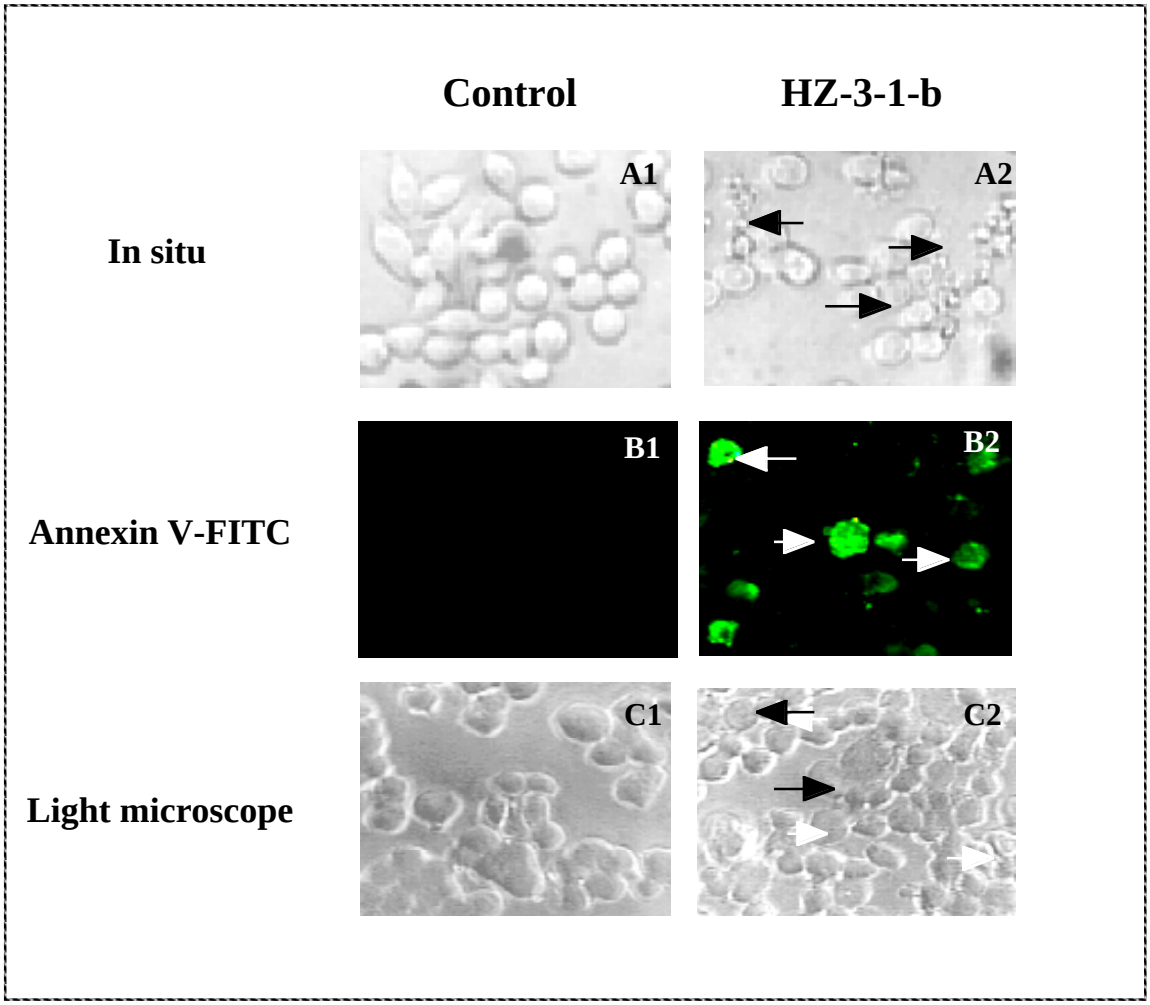


Fig. 26. Morphological changes of SW620 cells after treatment with HZ-3-1-b (10 µg/ml) for 24 h. The morphological changes of SW620 cells were observed microscopically in situ (A1, A2). After staining with annexin V-FITC conjugates, cells were analysed by fluorescence microscopy (B1, B2) and light microscopy (C1, C2). Arrows point to apoptotic cells.

Nuclear DNA fragmentation of SW620 cells was observed following treatment with 10 µg/ml HZ-3-1-b after 24 h. DNA content histograms obtained from PI-stained SW620 cells revealed that the percentage of cell population with reduced DNA content increased from 2.8% of the untreated cells to 10.0% of cells exposed to 10 µg/ml HZ-3-1-b for 24 h, 42.5% for 48 h and 55.3% for 72 h (Fig. 27). These observations indicate that after treatment with HZ-3-1-b for 72 h, more than half of SW620 cells were undergoing apoptosis.

The DNA fragmentation of SW620 cells was measured by flow cytometry. It was found that HZ-3-1-b induced apoptosis of SW620 cells in a dose and time-dependent manner. At the most effective concentration of 10 µg/ml, HZ-3-1-b induced more than 50% of the cells to undergo apoptosis after 72 h of exposure.

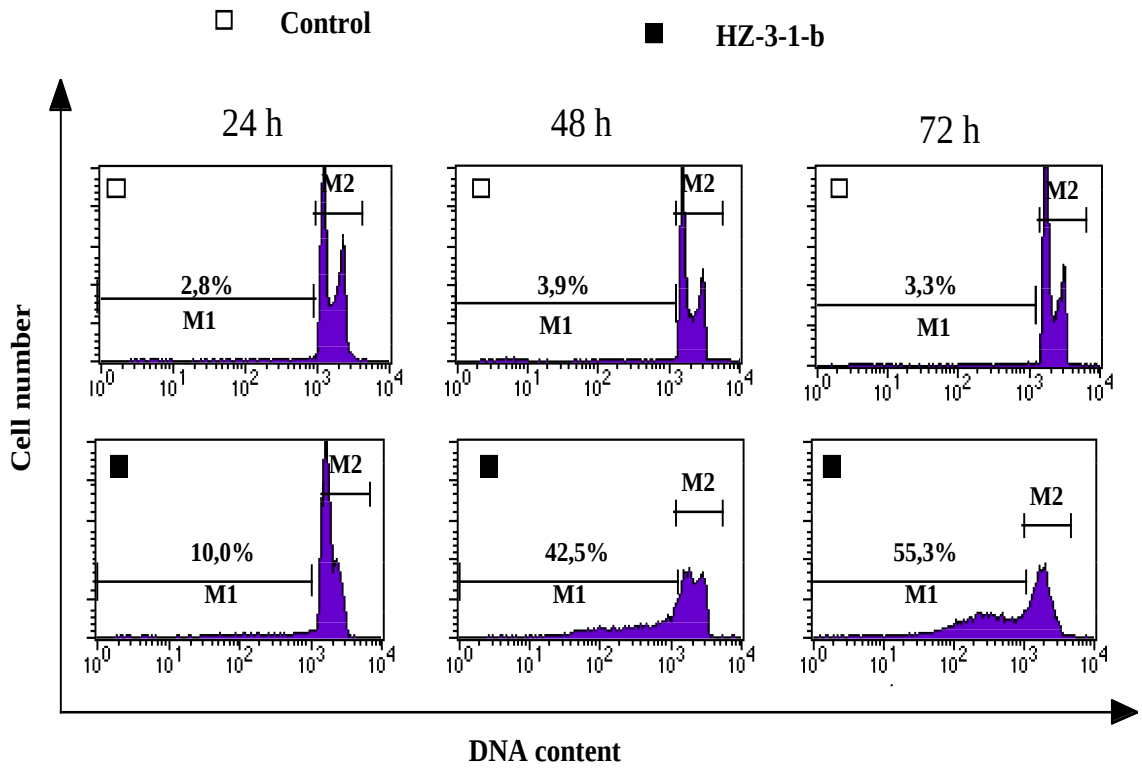


Fig. 27. Fragmentation of cellular DNA into oligonucleosomes. After SW620 cells were treated with HZ-3-1-b for 24 h, 48 h and 72 h, the DNA was stained with PI and analysed by flow cytometry. When the whole DNA was fragmented into oligonucleosomes, their fluorescence intensity will decrease along the DNA content axis compared with that of whole DNA, thus they shifted from M1 region to M2 region.

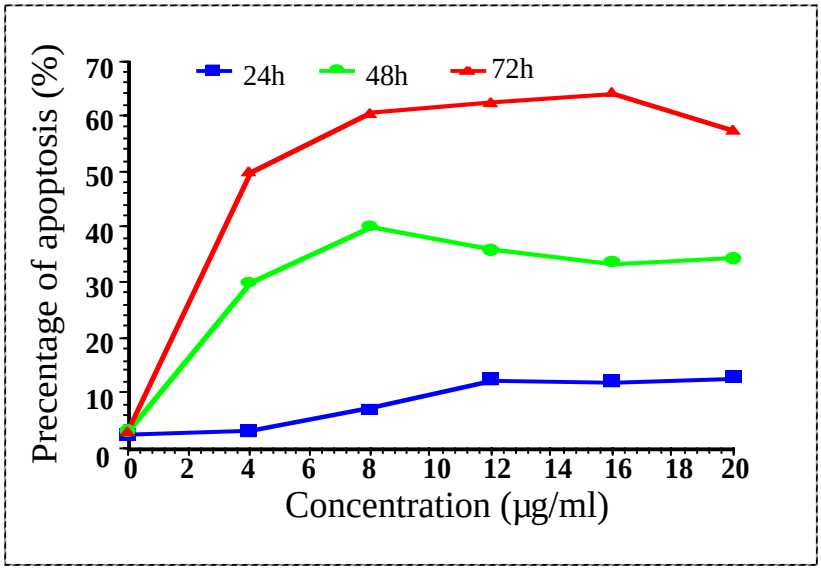


Fig. 28 Relationship between the apoptosis cells and the concentration of HZ-3-1-b in different times.

### 3.2.1.5. Influence of HZ-3-1-b on cell cycle of SW620 cells

In order to explore the basis of the anti-proliferation properties of the HZ-3-1-b, cell cycle analyses were performed. To examine the effect of HZ-3-1-b on SW620 cell cycle phase distribution (Fig. 29), SW620 cells were treated with HZ-3-1-b 10 μg/ml for different times. Compared with non-treated cells (0 h), the cells treated with HZ-3-1-b demonstrated an abnormal pattern of DNA profile. Cultivation of cells with HZ-3-1-b 10 μg/ml increased the population of SW620 cells in the S phase, while it decreased the population in G1 phase. A large proportion of the cells accumulated in S phase at 12 h and 24 h. These results suggest that SW620 cells were arrested in S phase after 24 h of treatment with HZ-3-1-b.

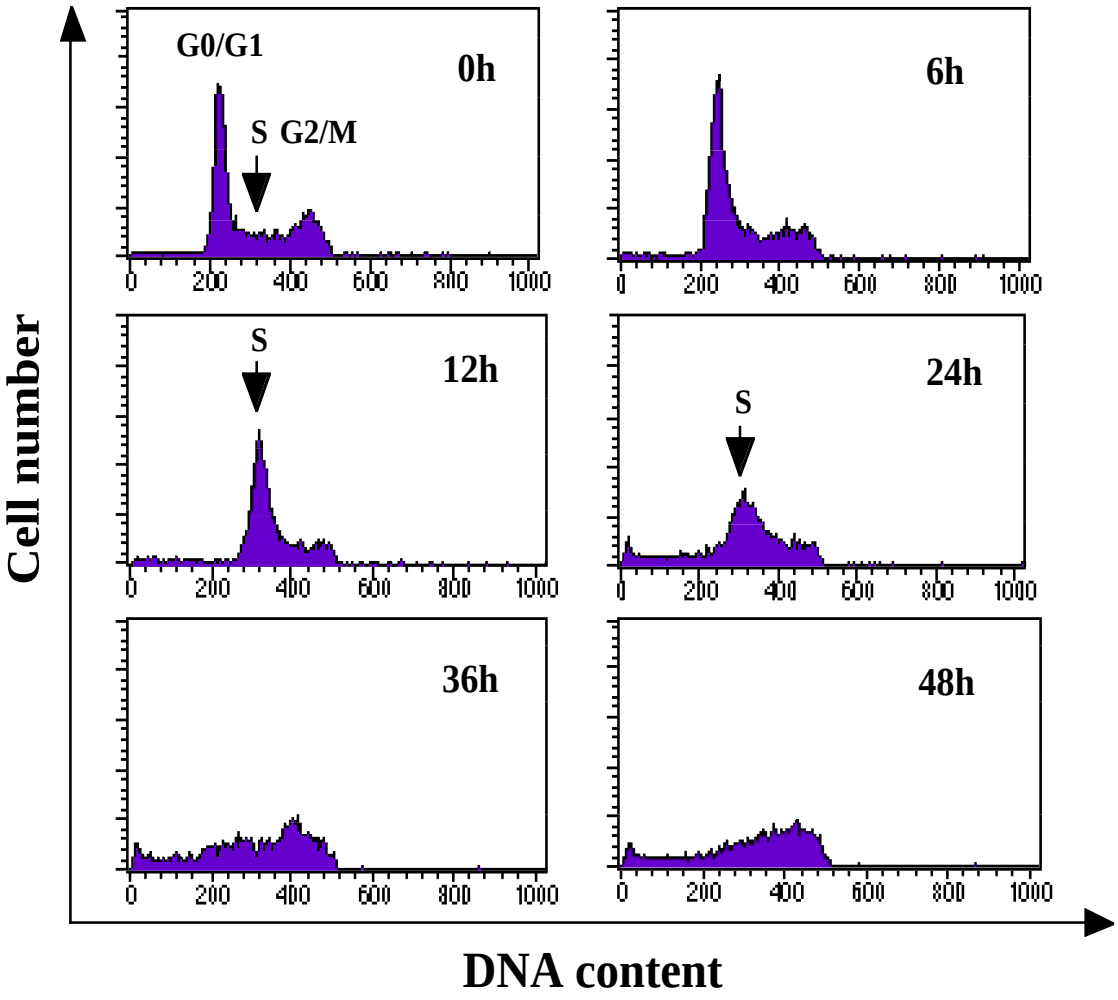


Fig. 29. Analysis of cell cycle arrest of SW620 cells after treatment with HZ-3-1-b. SW620 cells were treated with HZ-3-1-b (10 μg/ml) for different times. After collection, they were permeabilized and stained with PI, the percentage of cells in different phase of cell cycle was measured by FACScan.

## 3.2.2. Separation, purification and identification of the active compound from the crude extract of *Polygonum cuspidatum* in comparison with resveratrol

### 3.2.2.1. Fractionation of HZ by different methods

The dried ground roots of *polygonum cuspidatum* were extracted with boiling water, after vacuum evaporation of water, the crude extract of *polygonum cuspidatum*—HZ were obtained. The scheme of fractionation of the active compound from HZ is shown in Fig. 30.

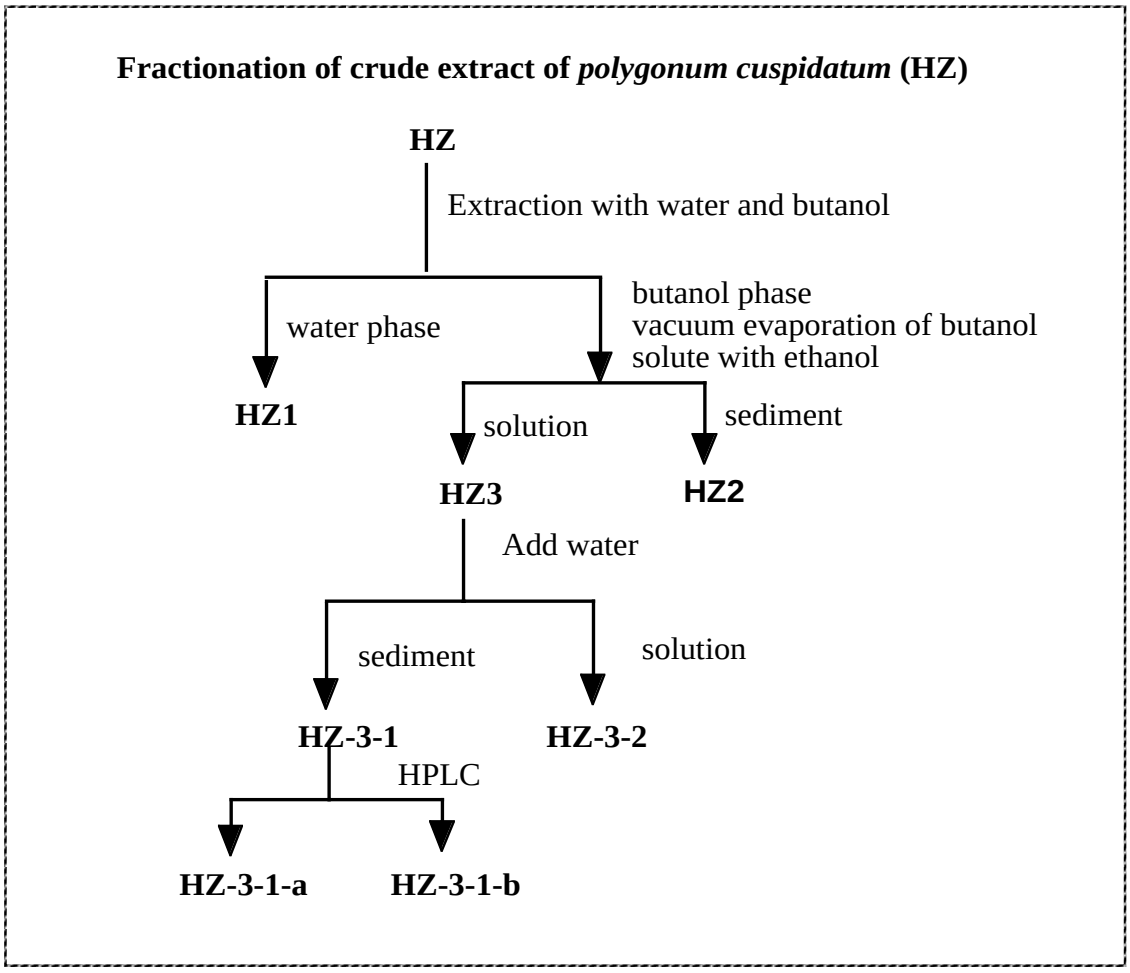


Fig. 30 Scheme of bioassay-guided fractionation of the crude extract of *Polygonum cuspidatum.*

HZ was fractionated to HZ-1, HZ-2 and HZ-3 according to partition between n-butanol and water and solubility in ethanol. Thin-layer chromatography (TLC) analysis showed that HZ-3, which exhibited strong inhibition capacity to tumour cells, had some clear points compared with HZ-1 and HZ-2 using UV detection. After the removal of more polar compounds from HZ-3, the fraction HZ-3-1 demonstrated more activity and contained fewer compounds (Fig. 31B).

Two main peaks were found when HZ-3-1 was checked by HPLC using reverse $C_{18}$ column (Fig. 31D). Five fractions were collected according to the indication in Fig. 31D and analysed by TLC. It was found that the fractions 2 and 4, which contained the peaks in HPLC, have one clear point detected by TLC (Fig. 31C). Through repeated purification using HPLC, two fractions, HZ-3-1-a (fraction 2) and HZ-3-1-b (fraction 4), which was only one peak analysed by HPLC, were achieved. Bioassay showed that the fraction HZ-3-1-b was more active than HZ-3-1-a (see 2.2.1. and Fig. 24C).

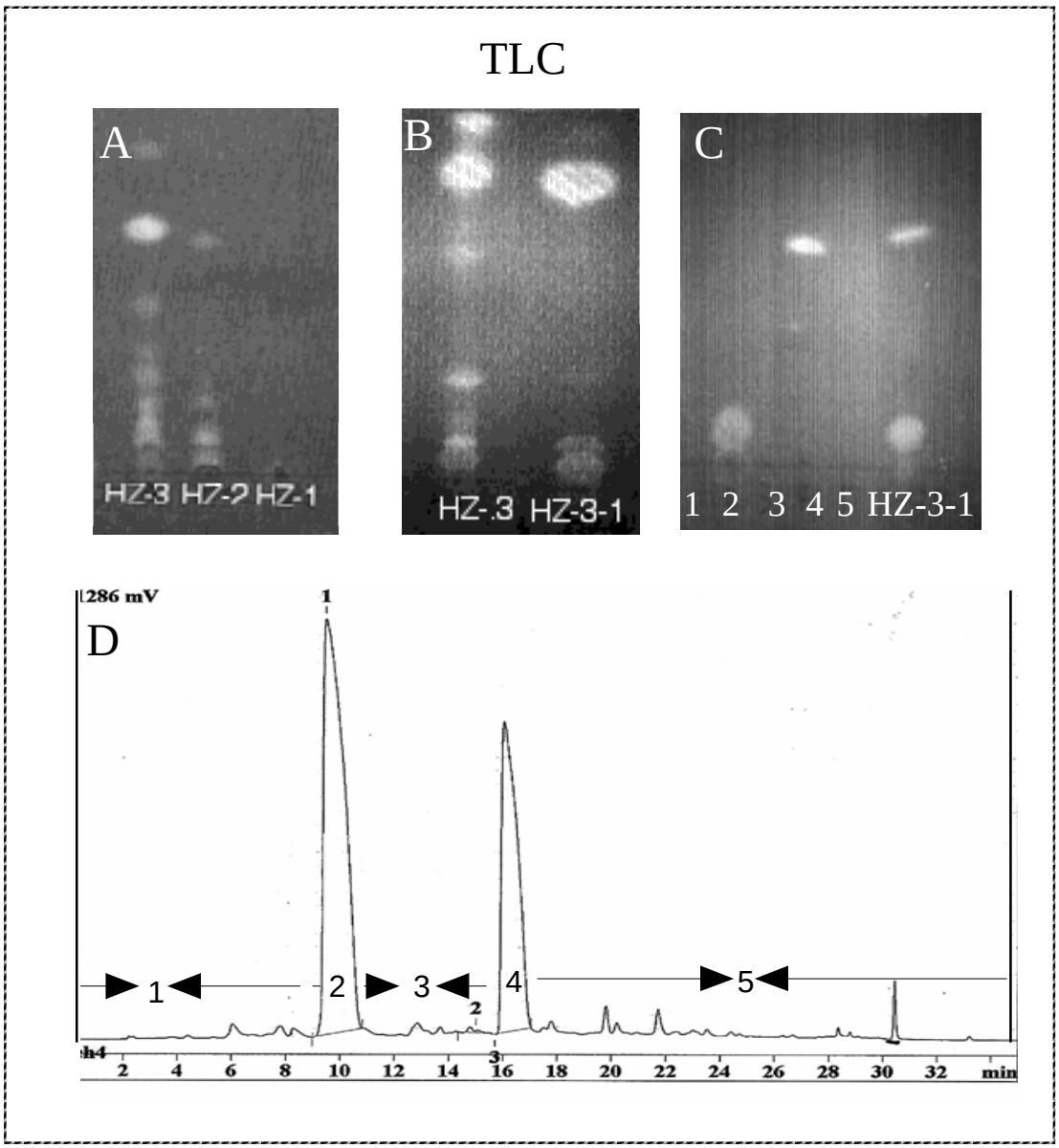


Fig. 31. Analysis of fractions and subfractions of HZ using thin-layer chromatography (TLC) and high-performance liquid chromatography (HPLC). (A) HZ-1, HZ-2 and HZ-3 (B) HZ-3 and HZ-3-1 (C) HPLC-fraction 1, 2, 3, 4, 5 were analysed on a plate of Silica gel $F_{254}$. It was detected using UV. (D) Fractionation of HZ-3-1 using HPLC, five fractions were collected according to the indication.

### 3.2.2.2. Identification of active compound HZ-3-1-b

The active compound HZ-3-1-b was purified from HZ, which exhibited only one point in TLC analysis and one peak in HPLC detected by UV light. This indicated the purity of the compound. The compound was first compared with compounds that were previously known in the plant *Polygonum cuspidatum.* HZ-3-1-b demonstrated remarkable peaks at 305 nm and 320 nm by UV scanning (Fig. 32A) and showed fluorescence under UV light detection. Among the various compounds in the plant, resveratrol also had characteristic UV lighting.

HZ-3-1-b was compared to resveratrol using UV, TLC and HPLC. The UV-Vis spectrum of HZ-3-1-b showed 305 nm and 320 nm of λmax in MeOH, which is in good agreement with resveratrol (Fig. 32A). Through TLC analysis, it was found that the Rf value of HZ-3-1-b was essentially identical with that of resveratrol (Fig. 32B), and the mixture of resveratrol and HZ-3-1-b also exhibited one point with the same Rf value. Reverse HPLC detection showed that the component HZ-3-1-b had the same retention time as resveratrol, and the mixture of HZ-3-1-b and resveratrol also demonstrated a single peak and the same retention time (Fig. 33). This data indicates that the active compound HZ-3-1-b and resveratrol were identical.

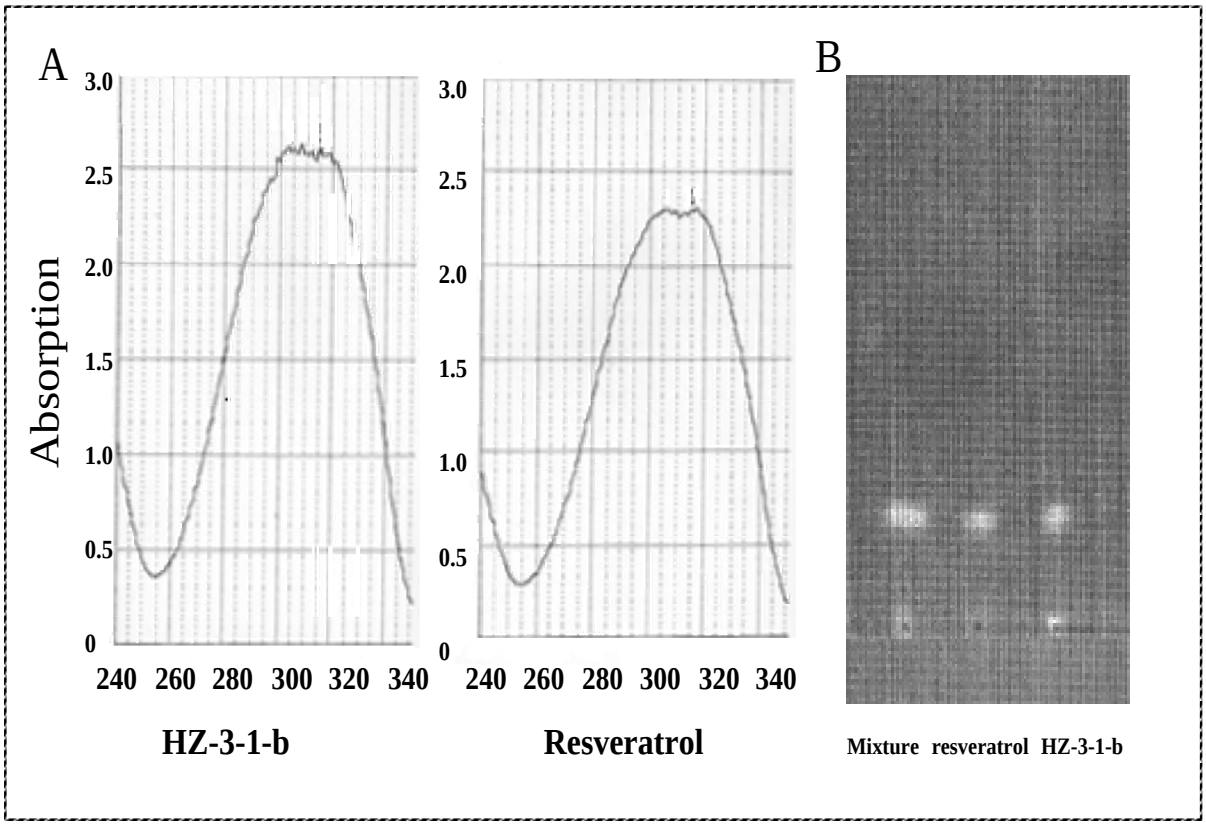


Fig. 32 UV-Vis spectrum and TLC of resveratrol and HZ-3-1-c. (A) Resveratrol and HZ-3-1-b were dissolved in ethanol and detect by UV scan from wave 240 nm to 340 nm. (B) Resveratrol, HZ-3-1-b and mixture of HZ-3-1-b and resveratrol were developed on Silica gel 254 with the ethyl acetate:petroleum ether = 9:1, and checked by UV detection.

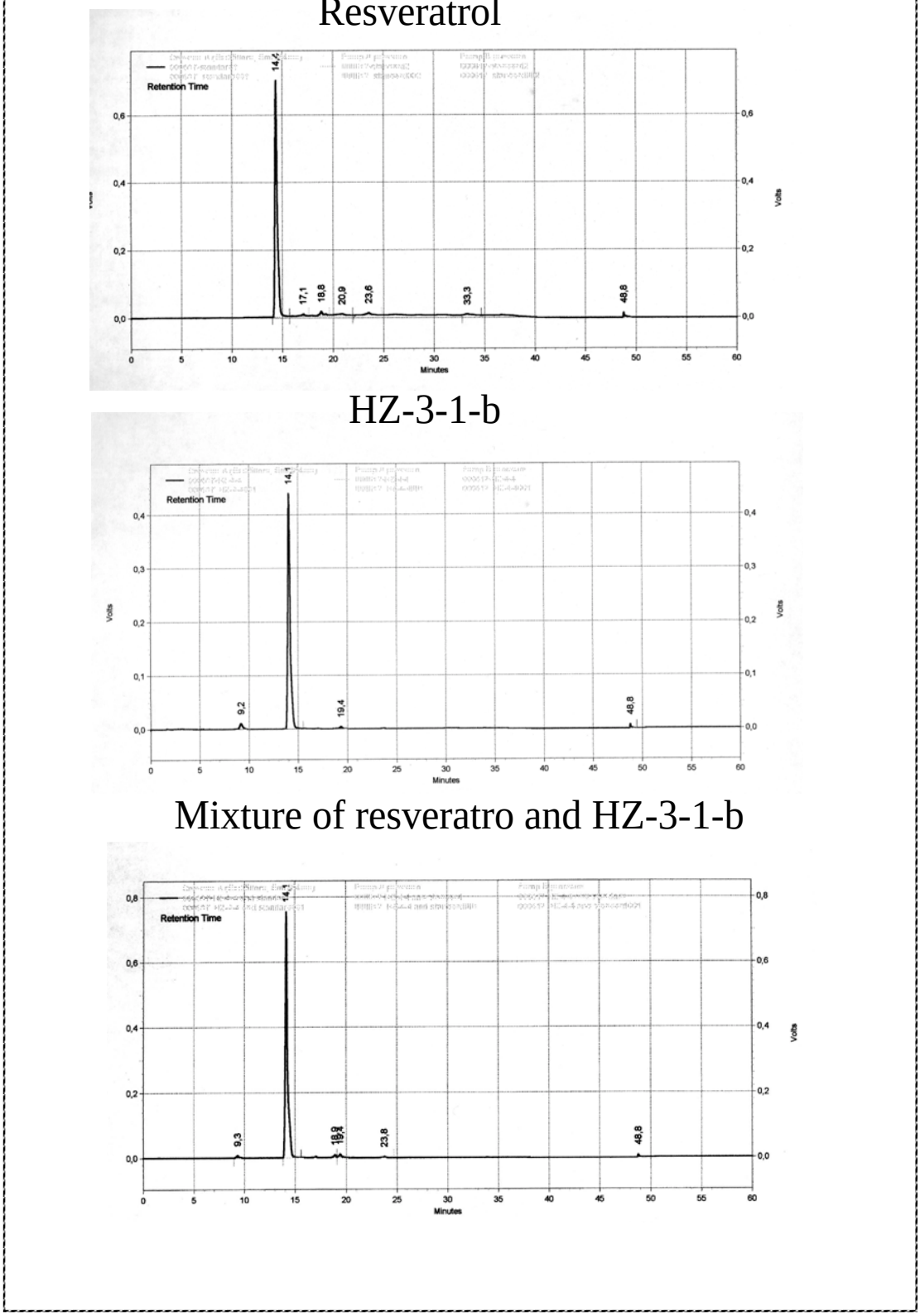


Fig. 33 HPLC of standard sample resveratrol (A), HZ-3-1-b (B) and mixture of resveratrol and HZ-3-1-b (C). The sample were analyzed by reversed-phase HPLC (Eurospher 100-$C_{18}$, 4.0 x 25 mm), elute with $H_2O$: Acetonitril = 10:90, flow rate 1 ml/min, temperature:25°C.

## 3.2.3. Binding of resveratrol (HZ-3-1-b) to glyceraldehyde-3-phosphate dehydrogenase (GAPDH) and inhibition by resveratrol of GAPDH enzyme activity

### 3.2.3.1. SDS-PAGE analysis of affinity purified sample by resveratrol-conjugated affinity chromatography

The results above demonstrate that HZ-3-1-b (resveratrol) is one of the active compounds in the plant *Polygonum cuspidatum*, and could inhibit growth of various tumour cells. Recently several papers reported that resveratrol could induce apoptosis (Lee et al., 2002; Sgambato et al., 2001; Sun ZJ et al., 2002), but the mechanism still remains unclear.

In order to isolate the targeting molecule of resveratrol, resveratrol conjugated affinity chromatography was used. SW620 and J774 cells were solubilized and loaded onto a resveratrol affinity sepharose column or sepharose column. The eluates were analysed by SDS-PAGE. The solubilisation of SW620 and J774 cells exhibited a great number of protein bands, while the eluates of SW620 and J774 cell solubilisations from the resveratrol conjugated affinity column exhibited only one band (Fig. 34). The band in both SW620 and J774 cells in SDS-PAGE demonstrated the same molecular weight, ca. 35-40 k. A sepharose column was done as a control; the eluates from sepharose columns showed no clear band. The results indicate that the protein isolated from resveratrol conjugated affinity columns is a major binding protein of resveratrol, which has a specific interaction with resveratrol.

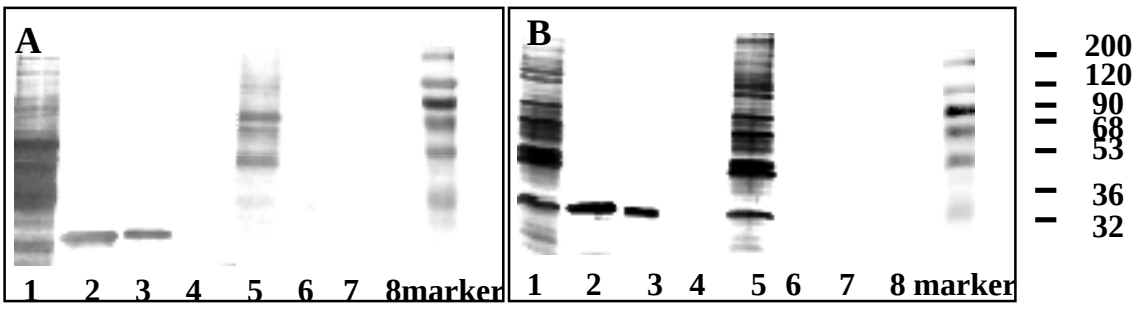


Fig. 34 SDS-PAGE analysis of eluates from resveratrol-conjugated affinity chromatography. Total cell lysates of SW620 (A) and J774 (B) were loaded onto resveratrol affinity columns or sepharose column and eluted with different buffer. The eluates were analysed by SDS-PAGE. Lane 2-4 were eluates from resveratrol affinity columns, lane 6-8 were eluates from sepharose colum,. lane1, 5 total protein of cell lysate; Lane 2,6 eluted with PBS buffer (pH 7.2); Lane 3, 7 eluted with glycin-HCl (pH 5.5); Lane 4, 8 eluated with glycin-HCl (pH 3.0).

### 3.2.3.2 Identification of resveratrol-binding protein by MALDI-TOF Mass Spectrometry

The eluates from the resveratrol conjugated column were separated by SDS-PAGE. The major band with 35-40 k was cut from SDS-PAGE and digested in the gel with trypsin. The peptide was analysed by MALDI-TOF mass spectrometry. One peptide peak with a molecular mass of 1762 was subjected to MALDI-PSD analysis. The fragment pattern compared to a

protein database indicated that these peptides belong to the protein GAPDH. For this database search, the mass tolerance from PSD data demonstrated that this protein was GAPDH. It has a molecular weight of 37 k.

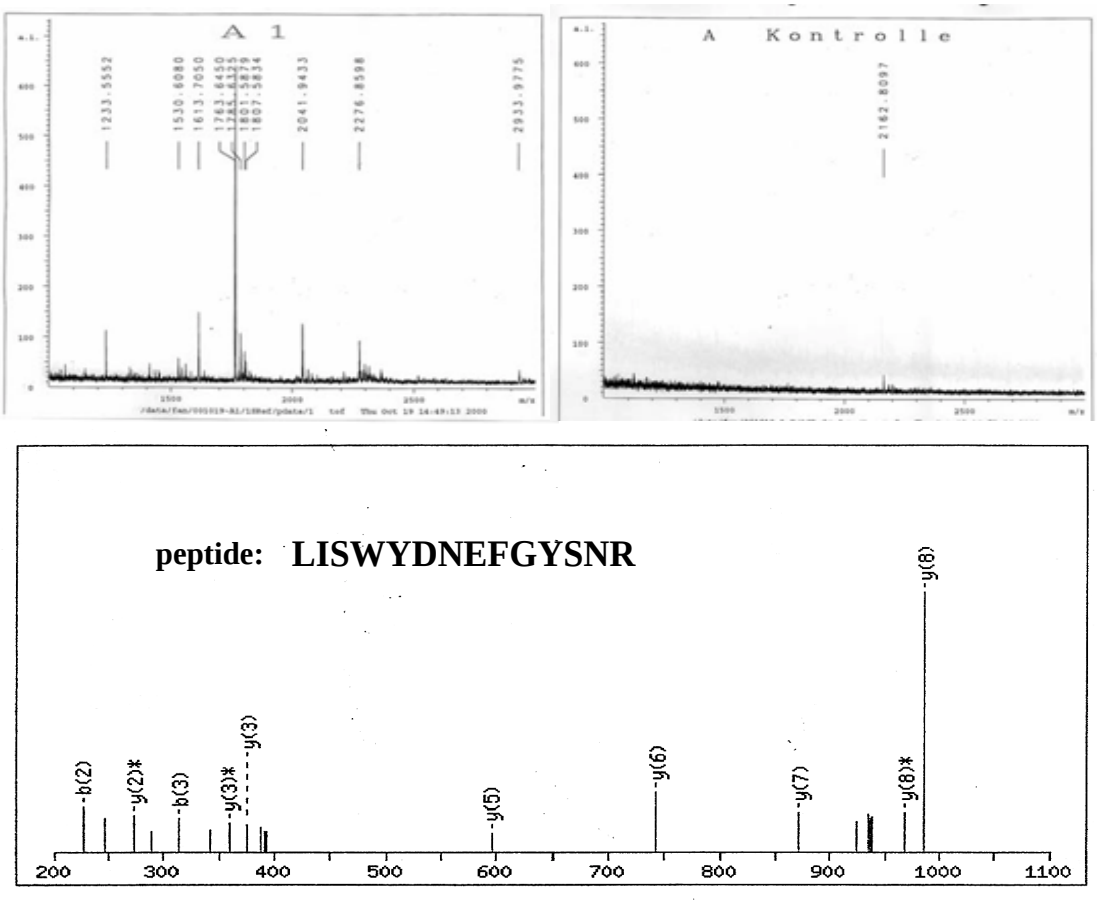


Fig. 35. MALDI-MS spectrum obtained in positive ion mode of the peptide mixture resulting from trypsin digest of the protein. The protein band (A) or the gel without band (B) for control were digested with trypsin and analysed by MALDI-MS. (C) MALDI-MS-PSD spectrum of the 1763 peptide. The fragment fit to the indicated peptide from GAPDH.

### 3.2.3.3. Inhibition of the GAPDH enzyme activity by resveratrol

GAPDH is a key enzyme of glycolysis. It could be demonstrated that enzyme activity was reduced in a dose dependent manner in the presence of resveratrol (Fig. 36A). With a high concentration of 100 µM, resveratrol inhibited the activity of GAPDH to 40%.

The effect of resveratrol on GAPDH enzyme activity was analysed kinetically. 50 µM resveratrol was added to the enzyme solution. The enzyme activity of GAPDH reached a plateau with or without resveratrol at 2 mM of Glyceraldehyde-3-phosphate (G-3-P) and was maintained at 5 mM and 10 mM, showing saturation of the enzyme with its substrate. However, the maximum activities were different. In the absence of resveratrol, the activity of GAPDH reached 800 U, whereas in the presence of resveratrol, the activity of GAPDH reached only 600 U. The double-reciprocal plot showed that $V_{max}$ was decreased by about

21%, while the $K_m$ of GAPDH remained unchanged in the presence of resveratrol. This suggests that resveratrol could inhibit the enzyme activity of GAPDH in a noncompetitive manner.

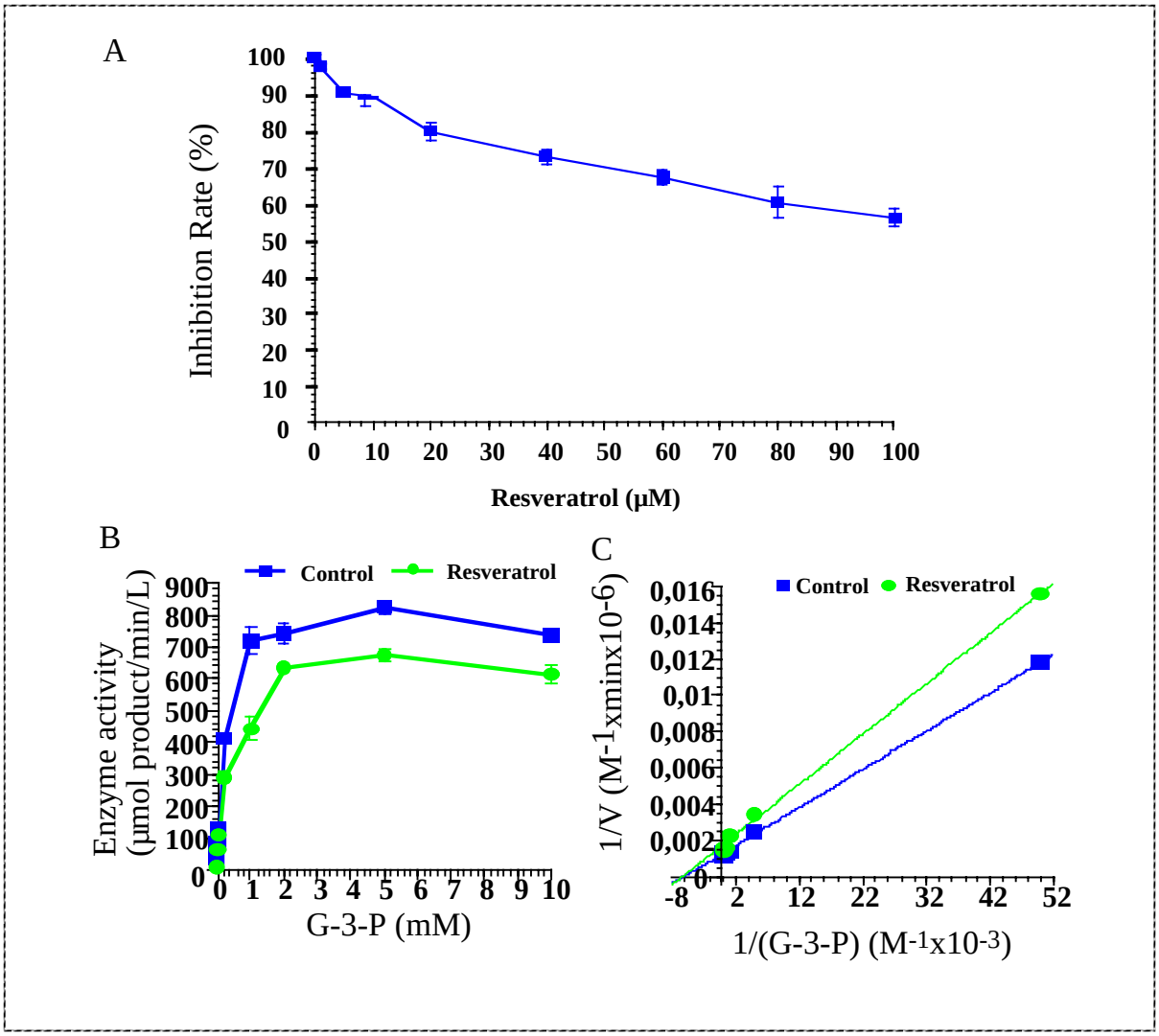


Fig. 36. Changes in GAPDH activity in presence or absence of resveratrol. (A) Enzyme activity of GAPDH was measured in presence of different concentration of resveratrol. (B) The activity of GAPDH (1µl, 10 µg) is plotted as a function of different substrate Glyceraldehyde-3-phosphate (G-3-P) concentration the final concentration of resveratrol is 50 µM. (C) Double-reciprocal plot of GAPDH activity in presence or absence of 50 µM resveratrol. Results present mean ± SD of triplicates of one representative experiments.